Prediction-Based Control for Mitigation of Axial–Torsional Vibrations in a Distributed Drill-String System

Shabnam Tashakori, Gholamreza Vossoughi, Hassan Zohoor, and Nathan van de Wouw, *Fellow, IEEE*

***Abstract*— This article proposes a control strategy to stabilize the axial–torsional dynamics of a distributed drill-string system. An infinite-dimensional model for the vibrational dynamics of the drill string is used as a basis for controller design. In this article, both the cutting process and frictional contact effects are considered in the bit–rock interaction model. Moreover, models for the top-side boundary conditions regarding axial and torsional actuation are considered. The resulting model is formulated in terms of neutral-type delay differential equations that involve constant state delays, state-dependent state delays, and constant input delays arising from the distributed nature of the drill-string dynamics and the cutting process at the bit. Using a spectral approach, the stability and stabilizability of the associated linearized dynamics are analyzed to support controller design. An optimization-based continuous pole-placement technique has been employed to design a stabilizing controller. Since the designed state-feedback control law needs state prediction, a predictor with observer structure is proposed. Both the controller and the predictor only employ top-side measurements. The effectiveness of the control strategy, in the presence of measurement noise, is shown in a representative case study. It is also shown that the controller is robust to parametric uncertainty in the bit–rock interaction.**

***Index Terms*— Continuous pole-placement method, distributed dynamics, drill-string dynamics, neutral-type time-delay (NTD) model, prediction-based control, spectral approach, stability analysis.**

I. Introduction

DRILLING systems are used for exploration and harvesting of oil, gas, and geothermal energy and suffer from complex coupled dynamics that involve axial, torsional, and lateral vibrations. Point contact between the drill string and the well-bore, mass imbalance, and downhole interactions are the main sources of these unwanted vibrations, which leads to the reduction of drilling efficiency, system failure, and rig downtime. The mitigation of these vibrations is hence of utmost importance.

Different approaches have been employed to model these vibrational phenomena: lumped-parameter models [1]–[3], distributed parameter models [4]–[6], and neutral-type time-delay (NTD) models [7]–[9]. NTD models strike a favorable balance between modeling accuracy and complexity of simulation, analysis, and control. Namely, these models are more accurate than lumped-parameter models since they do not neglect the distributed nature of the drill-string dynamics. Moreover, for such NTD models, a wide range of methods for stability analysis and control are available, compared to models in terms of partial differential equations (PDEs), while they involve less complexity in control design than distributed parameter models [10]. Such an internal NTD model is obtained directly from the distributed parameter model by neglecting the damping along the drill string. The NTD model was established in [7], [8], where the bit–rock interaction is modeled as a mere frictional contact, and modified in [9] with consideration of the cutting process as well as the frictional contact in the bit–rock interaction. A review of mathematical modeling of axial and torsional self-excited drilling vibrations can be found in [11].

To study the bit–rock interaction in drilling systems, several friction models have been employed [12], [13]. However, it has been shown in [14] that the bit–rock interaction consists of a cutting process and a frictional contact process, where the interaction between the drill-string dynamics and the delay nature of the cutting model leads to instability and self-excited oscillations. This time-delay effect is known as the root cause of such self-excited axial–torsional vibrations. The aforementioned bit–rock interaction model has been employed to study the drill-string vibrations in [5] and [15]–[19]. In this article, we will combine the infinite-dimensional NTD modeling approach with such bit–rock interaction model to arrive at an NTD model capturing both the distributed nature of the drill string and the cutting process at the bit.

The stability of vibrational models for drilling systems, including the state-dependent delay (induced by the cutting process in the bit–rock interaction), has been studied in [20]–[25] for finite-dimensional models and in [5] and [26] for distributed models. For NTD-type models, the exponential stability is investigated in [27] for a torsional model with

Manuscript received September 18, 2020; revised February 27, 2021; accepted March 2, 2021. Date of publication March 24, 2021; date of current version December 15, 2021. Manuscript received in final form March 10, 2021. Recommended by Associate Editor S. Pirozzi. *(Corresponding author: Gholamreza Vossoughi.)*

Shabnam Tashakori, Gholamreza Vossoughi, and Hassan Zohoor are with the Department of Mechanical Engineering, Sharif University of Technology, Tehran 11365-11155, Iran (e-mail: shabnam.tashakori@mech.sharif.edu; vossough@sharif.edu; zohoor@sharif.edu).

Nathan van de Wouw is with the Department of Mechanical Engineering, Eindhoven University of Technology, 5600 MB Eindhoven, The Netherlands, and also with the Department of Civil, Environmental and Geo-Engineering, University of Minnesota, Minneapolis, MN 55455 USA (e-mail: n.v.d.wouw@tue.nl).

Color versions of one or more figures in this article are available at https://doi.org/10.1109/TCST.2021.3065669.

Digital Object Identifier 10.1109/TCST.2021.3065669

considering only the frictional contact in the bit–rock interface. Here, we will pursue stability (and stabilizability) analysis for the novel NTD model to be proposed.

Vibrations of the drilling system are usually suppressed by adjusting surface-controlled variables (e.g., the hook force, the top-drive torque, and the characteristics of the drilling fluid). The controller design for mitigation of drilling torsional vibrations has been studied in [28]–[31] for finite-dimensional models and in [32]–[36] for infinite-dimensional models. The suppression of drilling axial–torsional vibrations has been studied in [17], [24], and [37] for lumped-parameter models, in [38] for distributed parameter models, in [39] for a coupled PDE-ordinary differential equation (ODE) model, and in [40]–[42] for NTD models. The Z-torque system of Shell [43] considers an infinite-dimensional model as a starting point and implements impedance matching in a practical way, but it still only considers the torsional dynamics. Besselink *et al.* [17] and Liu *et al.* [24] considered both the axial and torsional dynamics as a basis for controller design but employ a simple lumped-parameter model and hence also ignore the rich dynamics of the drill string. Vromen *et al.* [28], [29] took multiple modes into account for the controller design but still only consider the torsional dynamics and a finite-dimensional (discretized) model. Regarding the control of NTD models, a controller is designed in [40] based on the Lyapunov theory, aiming at suppressing stick-slip vibrations. Then, based on simulation results, it is concluded that it also mitigates the axial vibrations. The design of a PID controller to avoid axial–torsional vibrations is presented in [41]. Since the downhole data are received with some time delay, a delayed feedback controller is also designed. In [42], the flatness property of the drilling system is used to design a feedback controller, which eliminates both axial and torsional vibrations. Note that the NTD models in [40]–[42] do not consider the bit–rock interaction model mentioned in [14], which is considered essential in the root cause for drill-string vibrations. It is worth mentioning that employing NTD models for controller design serves as a worst case scenario since in-domain damping, which is neglected in these models, actually helps stabilization. Summarizing, many existing control strategies consider finite-dimensional models and hence ignore the inherent infinite-dimensional nature of the dynamics (see [17], [24]) and many control strategies consider only the stabilization of the torsional dynamics. Some examples are [4], [28], [29], and [36] and the industrial soft torque system [44].

In this article, an infinite-dimensional NTD model is employed and extended to study coupled axial–torsional vibrations. In comparison with previous studies, first, both the cutting process and frictional contact effects are taken into consideration in the bit–rock interaction model, and second, realistic top-side boundary conditions are included. More specifically, the high inertia of the torsional top drive is considered to regard the reflection of torsional waves at the top drive. Furthermore, instead of the hook load, the axial actuation is considered in terms of the velocity of the traveling block to which the drilling system is attached [45], [46]. Hence, this article presents a novel, extended NTD model for coupled axial–torsional drill-string dynamics. The resulting equations of motion are neutral-type delay differential equations (NDDEs) with constant input delays and constant state delays (both related to the wave propagation speeds along the drill string) and a state-dependent state delay (induced by the bit–rock interaction). Then, a spectral approach is employed to analyze the stability of the associated linearized dynamics to study the root causes of the steady-state vibrations and to serve as a basis for controller design. Moreover, with an input transformation (i.e., precompensators), the system is rendered to be "formally stable" and "spectrally stabilizable" [47] such that the stabilizability (by state feedback) of the system dynamics is guaranteed. Next, to design the controller, the optimization-based continuous pole-placement method [48] has been employed, aiming at eliminating both axial and torsional vibrations. Then, to render the control strategy causal, a predictor with observer structure is designed to complement the state-feedback controller. Note that the generic controller and predictor design methodologies have been previously presented in the delay systems literature, but in this article, they are employed for the first time to solve a stabilization control problem for drilling systems.

The main contribution of this article is the design of a prediction-based state-feedback controller, mitigating the coupled axial–torsional drill-string vibrations while dealing with the infinite-dimensional dynamics of the drill string and the associated constant state delays and input delays and the state-dependent delay effect induced by the bit–rock interaction. Additional contributions of this article are that the designed controller, first, guarantees asymptotic stability of the desired solution, second, is compatible with the top-drive actuator limitations, third, only employs top-side measurements, fourth, is robust to measurement noise, and, fifth, is robust to parametric uncertainty in the bit–rock interaction. Moreover, an illustrative case study is presented to show the effectiveness of both the controller and the predictor.

Existing control strategies come at many levels of complexity (simple PI control, impedance matching, H_∞-based dynamic controllers, and other wave-based control approaches [43], [49], [50]). Note that although the strategy introduced in this article is more involved than some previously presented controllers, it is still feasible for practical implementation. The additional complexity is motivated by the fact that it provides the possibility of dealing with the complex, coupled axial–torsional and infinite-dimensional dynamics of the drill-string system. This is important, first, as the interaction between the axial and torsional dynamics is key in the stability of the drilling system (see [14]) and, second, as higher order modes can induce instability and a (simpler) control approach may not be able to mitigate drill-string vibrations (see [29], [51]).

This article is organized as follows. Section II introduces the distributed model describing the axial and torsional drill-string dynamics. Subsequently, the associated linearized dimensionless perturbation dynamics is presented. The stability properties of the open-loop system are analyzed in Section IV. Moreover, the stabilizability of the system is studied. Section V presents the controller design. To make the resulting controller causal, a predictor is designed in Section VI. Illustrative simulation results are presented in

Section VII, where the robustness of the designed controller against parametric uncertainties is also analyzed. Finally, conclusions are presented in Section VIII.

II. Distributed Drill-String Model

To the best of authors' knowledge, expressing the oscillatory behavior of the drilling system by using the following wave equations was first presented in [52], [53]:

$$\frac{\partial^2 U}{\partial s^2}(s,t) = c_a^2 \frac{\partial^2 U}{\partial t^2}(s,t) \tag{1a}$$

$$\frac{\partial^2 \theta}{\partial s^2}(s,t) = c_t^2 \frac{\partial^2 \theta}{\partial t^2}(s,t) \tag{1b}$$

where $U(s,t)$ and $\theta(s,t)$ are the axial and angular positions along the drill string with the spatial variable $s \in [0, L]$ (with L the drill-string length) and time t (see Fig. 1), respectively. The wave velocity constants in (1) are given by

$$c_a = \sqrt{\frac{\rho}{E}}, \quad c_t = \sqrt{\frac{\rho}{G}} \tag{2}$$

where ρ, E, and G are, respectively, the density, Young modulus, and shear modulus of drilling pipes (see Table I). Based on the above wave equation model, the following relations between the downhole and top-side velocities hold (see [54]):

$$\frac{\partial U_b}{\partial t}(t-\tau_a) = \frac{1}{2}\Bigg(\frac{\partial U_{\text{top}}}{\partial t}(t) + \frac{1}{c_a}\frac{\partial U_{\text{top}}}{\partial s}(t) + \frac{\partial U_{\text{top}}}{\partial t}(t-2\tau_a) - \frac{1}{c_a}\frac{\partial U_{\text{top}}}{\partial s}(t-2\tau_a)\Bigg) \tag{3a}$$

$$\frac{\partial \theta_b}{\partial t}(t-\tau_t) = \frac{1}{2}\Bigg(\frac{\partial \theta_{\text{top}}}{\partial t}(t) + \frac{1}{c_t}\frac{\partial \theta_{\text{top}}}{\partial s}(t) + \frac{\partial \theta_{\text{top}}}{\partial t}(t-2\tau_t) - \frac{1}{c_t}\frac{\partial \theta_{\text{top}}}{\partial s}(t-2\tau_t)\Bigg) \tag{3b}$$

where

$$U_{\text{top}}(t) := U(0,t), \quad U_b(t) := U(L,t) \tag{4a}$$

$$\theta_{\text{top}}(t) := \theta(0,t), \quad \theta_b(t) := \theta(L,t). \tag{4b}$$

The time delays in (3) (τ_a and τ_t) are, respectively, the time required for the axial and torsional waves to travel from one extremity of the drill string to the other, which are defined as

$$\tau_a = c_a L, \quad \tau_t = c_t L. \tag{5}$$

These time delays can be assumed constant since the drill-string length is quasi-constant on the relevant vibrational time scale.

The boundary conditions for the axial and torsional dynamics are given by

$$\frac{\partial U_{\text{top}}}{\partial t}(t) = V_{\text{TB}}(t) \tag{6a}$$

$$E\Gamma \frac{\partial U_b}{\partial s}(t) = -M_B \frac{\partial^2 U_b}{\partial t^2}(t) - W(t) \tag{6b}$$

and

$$GJ\frac{\partial \theta_{\text{top}}}{\partial s}(t) = I_T \frac{\partial^2 \theta_{\text{top}}}{\partial t^2}(t) + \beta \frac{\partial \theta_{\text{top}}}{\partial t}(t) - u_T(t) \tag{7a}$$

$$GJ\frac{\partial \theta_b}{\partial s}(t) = -I_B \frac{\partial^2 \theta_b}{\partial t^2}(t) - T(t) \tag{7b}$$

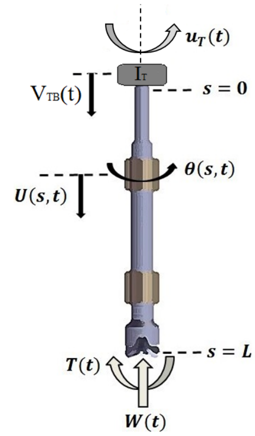

Fig. 1. Schematic of the drill string.

TABLE I
Model Parameters [14], [40], [42]

Parameter	Definition	Value
M_B	BHA mass	40000 kg
I_B	BHA moment of inertia	89 kgm^2
I_T	Top-drive moment of inertia	79 kgm^2
E	Young modulus	200×10^9 N/m^2
G	Shear modulus	79.3×10^9 N/m^2
ρ	Density	8000 kg/m^3
Γ	Drill pipe cross sectional area	35×10^{-4} m^2
J	Drill pipe polar moment of area	1.19×10^{-5} m^4
L	Drill string length	1172 m
α, β	Viscous friction coefficients	200.025 kg/s, 2000 Nms
ε	Rock intrinsic specific energy	60×10^6 N/m^2
a	Bit radius	10.8×10^{-2} m
ζ	Cutter face inclination number	0.6
σ	Maximum contact pressure at the wearflat-rock interface	60×10^6 Pa
l	Length of the drill bit wearflat	1.2×10^{-3} m
μ	Coefficient of friction at the wearflat-rock interface	0.6
γ	Bit geometry number	1
n	Number of blades	4

respectively, where Γ and J are, respectively, the drill pipe cross-sectional area and polar moment of area, M_B and I_B specify the bottom hole assembly (BHA) inertial characteristics, I_T is the top-drive moment of inertia, and α and β characterize the viscous friction at the top drive (see Table I).

The traveling block is an arrangement of pulleys or sheaves, whereby the drilling line is reeved. This block can move (axially) up and down freely and, together with the crown block and the drill line, facilitates lifting the drill string. The axial velocity of the traveling block V_{TB} (i.e., the feed rate) [46] in (6a) and the top-drive torque u_T in (7a) are the control inputs, both exerted at the rig (see Fig. 1).

Let us introduce the following input transformation in support of the stabilizing controller design, pursued in

Section V:

$$u_1(t) = \alpha V_{\mathrm{TB}}(t) - E\Gamma \frac{\partial U_{\mathrm{top}}}{\partial s}(t) \tag{8a}$$

$$u_2(t) = u_T(t) - I_T \frac{\partial^2 \theta_{\mathrm{top}}}{\partial t^2}(t) \tag{8b}$$

where $u_1(t)$ and $u_2(t)$ are the new control inputs and $E\Gamma(\partial U_{\mathrm{top}})/(\partial s)(t)$ and $I_T(\partial^2\theta_{\mathrm{top}})/(\partial t^2)(t)$ are precompensators. The axial precompensator $E\Gamma(\partial U_{\mathrm{top}})/(\partial s)(t)$ is available as a measured output by the saver sub force measurement. The torsional precompensator $I_T(\partial^2\theta_{\mathrm{top}})/(\partial t^2)(t)$ is also available as the top-side acceleration can be obtained by differentiating the top-side velocity, which is itself available by measurement. Given (8), the top-side boundary conditions (6a) and (7a) can be rewritten in terms of new control inputs as follows:

$$E\Gamma \frac{\partial U_{\mathrm{top}}}{\partial s}(t) = \alpha \frac{\partial U_{\mathrm{top}}}{\partial t}(t) - u_1(t) \tag{9a}$$

$$GJ \frac{\partial \theta_{\mathrm{top}}}{\partial s}(t) = \beta \frac{\partial \theta_{\mathrm{top}}}{\partial t}(t) - u_2(t). \tag{9b}$$

On the other extremity, i.e., at the bit, W and T are the resistive force and torque applied from the formation to the bit, called weight-on-bit (WOB) and torque-on-bit (TOB), respectively (see Fig. 1). These are modeled by the following bit–rock interaction law [9], [24]:

$$W_c = \varepsilon a \zeta \mathbf{R}(d(t))\mathbf{H}(\dot{\theta}_b(t)) \tag{10a}$$

$$W_f = \sigma a l \mathbf{H}(d(t))\mathbf{H}(\dot{U}_b(t)) \tag{10b}$$

$$T_c = \frac{1}{2}\varepsilon a^2 \mathbf{R}(d(t))\mathbf{H}(\dot{\theta}_b(t)) \tag{10c}$$

$$T_f = \frac{1}{2}\mu\gamma a^2 \sigma l \mathbf{Sign}(\dot{\theta}_b(t))\mathbf{H}(d(t))\mathbf{H}(\dot{U}_b(t)) \tag{10d}$$

where the subscripts c and f denote the cutting components and friction components of the bit–rock interaction, respectively. The parameters $\varepsilon, a, \zeta, \sigma, l, \mu$, and γ in (10) characterize bit and rock properties, defined in Table I. The depth of cut $d(t)$, used in (10), is given by

$$d(t) = n(U_b(t) - U_b(t - \tau_n(t))) \tag{11}$$

for a n-blade bit, where the state-dependent delay $\tau_n(t)$ is the time that takes for the bit to rotate by the angle of $2\pi/n$. The delay $\tau_n(t)$ is state-dependent and governed by

$$\theta_b(t) - \theta_b(t - \tau_n(t)) = \frac{2\pi}{n}. \tag{12}$$

Nonlinear functions $\mathbf{R}(.)$, $\mathbf{H}(.)$, and $\mathbf{Sign}(.)$ in (10) are defined as follows:

$$\mathbf{R}(y) = \begin{cases} y, & y \geq 0 \\ 0, & y < 0 \end{cases} \tag{13a}$$

$$\mathbf{H}(y) = \begin{cases} 1, & y \geq 0 \\ 0, & y < 0 \end{cases} \tag{13b}$$

$$\mathbf{Sign}(y) = \begin{cases} \mathrm{sign}(y), & y \neq 0 \\ [-1, 1], & y = 0 \end{cases} \tag{13c}$$

which describes the following cases of drilling [15].

1) *Normal Cutting ($d > 0, \dot{U}_b > 0$, and $\dot{\theta}_b > 0$):* All the cutting and friction components of the bit–rock interaction are nonzero, which leads to the following bit–rock interaction law:

$$W(t) = \varepsilon a \zeta d(t) + \sigma a l \tag{14a}$$

$$T(t) = \frac{1}{2}\varepsilon a^2 d(t) + \frac{1}{2}\mu\gamma a^2 \sigma l. \tag{14b}$$

2) *Bit Bouncing ($d > 0, \dot{U}_b < 0$, and $\dot{\theta}_b > 0$):* The friction components of both WOB and TOB are zero since there is no contact between the bit and well-bottom.
3) *Reverse Rotation ($d > 0, \dot{U}_b > 0$, and $\dot{\theta}_b < 0$):* There is no cutting although the bit is in contact with the formation. Therefore, the cutting components are zero.
4) *Bit Off-Bottom ($d < 0$):* There is no contact between the bit and the formation, which leads to $W = T = 0$.

The NTD model is obtained directly from the wave equation model, given in (1), the top-side boundary conditions, given in (9), and bottom-side boundary conditions, given in (6b) and (7b), by employing Riemann variables, defined by

$$\Upsilon_a = t + c_a s, \quad \Lambda_a = t - c_a s \tag{15}$$

for the axial dynamics and by

$$\Upsilon_t = t + c_t s, \quad \Lambda_t = t - c_t s \tag{16}$$

for the torsional dynamics. Consequently, the solutions of undamped axial and torsional wave equations are decomposed as follows in these Riemann variables:

$$U(s,t) = \mathbf{f}_a(\Upsilon_a) + \mathbf{g}_a(\Lambda_a) \tag{17a}$$

$$\theta(s,t) = \mathbf{f}_t(\Upsilon_t) + \mathbf{g}_t(\Lambda_t) \tag{17b}$$

where $\mathbf{f}_i$ and $\mathbf{g}_i$, $i \in \{a, t\}$, are arbitrary functions correspond to uptraveling and downtraveling waves, respectively, with subscripts a and t the axial and torsional dynamics. With the use of (4), (5), and [15]–[17], the downhole velocities can be expressed as

$$\dot{U}_b(t) = \frac{\partial \mathbf{f}_a}{\partial \Upsilon_a}(t + \tau_a) + \frac{\partial \mathbf{g}_a}{\partial \Lambda_a}(t - \tau_a) \tag{18a}$$

$$\dot{\theta}_b(t) = \frac{\partial \mathbf{f}_t}{\partial \Upsilon_t}(t + \tau_t) + \frac{\partial \mathbf{g}_t}{\partial \Lambda_t}(t - \tau_t). \tag{18b}$$

Along the line of [9], the procedure of obtaining the axial and torsional NTD models is explained in the following.

A. Axial NTD Model

The axial boundary conditions, (9a) and (6b), can be, respectively, reformulated in terms of Riemann variables by using (17a) as follows:

$$(E\Gamma c_a - \alpha)\frac{\partial \mathbf{f}_a}{\partial \Upsilon_a}(t) - (E\Gamma c_a + \alpha)\frac{\partial \mathbf{g}_a}{\partial \Lambda_a}(t) = -u_1(t) \tag{19a}$$

$$E\Gamma c_a\left(\frac{\partial \mathbf{f}_a}{\partial \Upsilon_a}(t + \tau_a) - \frac{\partial \mathbf{g}_a}{\partial \Lambda_a}(t - \tau_a)\right) = -M_B \ddot{U}_b(t) - W(t). \tag{19b}$$

Equations (19b) and (18a) can be solved for $(\partial \mathbf{f}_a)/(\partial \Upsilon_a)(t+\tau_a)$ and $(\partial \mathbf{g}_a)/(\partial \Lambda_a)(t-\tau_a)$. After time shifting, the following equations hold:

$$\frac{\partial \mathbf{f}_a}{\partial \Upsilon_a}(t) = \frac{1}{2}\left(-\frac{M_B}{E\Gamma c_a}\ddot{U}_b(t-\tau_a) + \dot{U}_b(t-\tau_a) - \frac{1}{E\Gamma c_a}W(t-\tau_a)\right) \tag{20a}$$

$$\frac{\partial \mathbf{g}_a}{\partial \Lambda_a}(t) = \frac{1}{2}\left(\frac{M_B}{E\Gamma c_a}\ddot{U}_b(t+\tau_a) + \dot{U}_b(t+\tau_a) + \frac{1}{E\Gamma c_a}W(t+\tau_a)\right). \tag{20b}$$

Substituting (20) into (19a) ultimately leads to

$$\begin{aligned}\ddot{U}_b(t) - \bar{A}\ddot{U}_b(t-2\tau_a) = {} & -\bar{B}\dot{U}_b(t) - \bar{A}\bar{B}\dot{U}_b(t-2\tau_a) \\ & - \frac{1}{M_B}W(t) + \frac{1}{M_B}\bar{A}W(t-2\tau_a) \\ & + \bar{C}u_1(t-\tau_a)\end{aligned} \tag{21}$$

where

$$\bar{A} = \frac{\alpha - c_a E\Gamma}{\alpha + c_a E\Gamma}, \quad \bar{B} = \frac{c_a E\Gamma}{M_B}, \quad \bar{C} = \frac{2\bar{B}}{\alpha + c_a E\Gamma}. \tag{22}$$

Substituting the (linearized) bit–rock interaction law (14a), which is valid as we aim to (locally) stabilize a nominal drilling solution with the "normal cutting" regime, the depth of cut (11) in (21) gives

$$\begin{aligned}&\ddot{U}_b(t) - \bar{A}\ddot{U}_b(t-2\tau_a) \\ &= -\bar{B}\dot{U}_b(t) - \bar{A}\bar{B}\dot{U}_b(t-2\tau_a) - \frac{1}{M_B}\sigma a l\big(1-\bar{A}\big) \\ &- \frac{1}{M_B}\varepsilon a\zeta n(U_b(t) - U_b(t-\tau_n(t))) \\ &+ \frac{1}{M_B}\bar{A}\varepsilon a\zeta n(U_b(t-2\tau_a) - U_b(t-2\tau_a-\tau_n(t-2\tau_a))) \\ &+ \bar{C}u_1(t-\tau_a).\end{aligned} \tag{23}$$

B. Torsional NTD Model

Reformulating the torsional boundary conditions, (9b) and (7b), in terms of Riemann variables (17b), respectively, gives

$$(GJc_t - \beta)\frac{\partial \mathbf{f}_t}{\partial \Upsilon_t}(t) - (GJc_t + \beta)\frac{\partial \mathbf{g}_t}{\partial \Lambda_t}(t) = -u_2(t) \tag{24a}$$

$$GJc_t\left(\frac{\partial \mathbf{f}_t}{\partial \Upsilon_t}(t+\tau_t) - \frac{\partial \mathbf{g}_t}{\partial \Lambda_t}(t-\tau_t)\right) = -I_B\ddot{\theta}_b(t) - T(t). \tag{24b}$$

Solving (24b) and (18b) for $(\partial \mathbf{f}_t)/(\partial \Upsilon_t)(t+\tau_t)$ and $(\partial \mathbf{g}_t)/(\partial \Lambda_t)(t-\tau_t)$ and shifting time leads to the following relations:

$$\frac{\partial \mathbf{f}_t}{\partial \Upsilon_t}(t) = \frac{1}{2}\left(-\frac{I_B}{GJc_t}\ddot{\theta}_b(t-\tau_t) + \dot{\theta}_b(t-\tau_t) - \frac{1}{GJc_t}T(t-\tau_t)\right) \tag{25a}$$

$$\frac{\partial \mathbf{g}_t}{\partial \Lambda_t}(t) = \frac{1}{2}\left(\frac{I_B}{GJc_t}\ddot{\theta}_b(t+\tau_t) + \dot{\theta}_b(t+\tau_t) + \frac{1}{GJc_t}T(t+\tau_t)\right). \tag{25b}$$

Substituting (25) into (24a) gives the NTD model for the torsional dynamics as follows:

$$\begin{aligned}\ddot{\theta}_b(t) - A\ddot{\theta}_b(t-2\tau_t) = {} & -B\dot{\theta}_b(t) - AB\dot{\theta}_b(t-2\tau_t) \\ & - \frac{1}{I_B}T(t) + \frac{1}{I_B}AT(t-2\tau_t) \\ & + Cu_2(t-\tau_t)\end{aligned} \tag{26}$$

where

$$A = \frac{\beta - c_t GJ}{\beta + c_t GJ}, \quad B = \frac{c_t GJ}{I_B}, \quad C = \frac{2B}{\beta + c_t GJ}. \tag{27}$$

Substituting the (linearized) bit–rock interaction law (14b), which is valid as we aim to (locally) stabilize a nominal drilling solution with the "normal cutting" regime, the depth of cut (11) in (26) gives

$$\begin{aligned}&\ddot{\theta}_b(t) - A\ddot{\theta}_b(t-2\tau_t) \\ &= -B\dot{\theta}_b(t) - AB\dot{\theta}_b(t-2\tau_t) - \frac{1}{2I_B}\mu\gamma a^2\sigma l(1-A) \\ &- \frac{1}{2I_B}\varepsilon a^2 n(U_b(t) - U_b(t-\tau_n(t))) \\ &+ \frac{1}{2I_B}A\varepsilon a^2 n(U_b(t-2\tau_t) - U_b(t-2\tau_t-\tau_n(t-2\tau_t))) \\ &+ Cu_2(t-\tau_t).\end{aligned} \tag{28}$$

The NTD model, given in (23) and (28), is in the form of an NDDE with several state delays and input delays.

Reformulating the PDE model into a DDE model benefits the control design by opening up the opportunities for using controller synthesis tools for delay systems [10].

C. Dimensionless Perturbation Dynamics

The steady-state response of the model in (23) and (28) for nominal constant inputs, u_{1s} and u_{2s}, is defined as

$$U_b(t) = U_s(t) := V_0 t + U_0, \quad \dot{U}_s = V_0 \tag{29a}$$

$$\theta_b(t) = \theta_s(t) := \Omega_0 t + \theta_0, \quad \dot{\theta}_s = \Omega_0 \tag{29b}$$

where V_0 and Ω_0 are the nominal penetration rate and nominal rotational velocity of the bit, which physically represent the desired drilling response without vibrations. Substituting (29) into (23) and (28) gives the following relations between the nominal speeds and nominal constant control inputs, associated with the steady-state response in (29):

$$\begin{aligned}V_0\bar{B}\big(1+\bar{A}\big) = {} & -\frac{1}{M_B}\varepsilon a\zeta n\big(1-\bar{A}\big)V_0\tau_{n0} \\ & - \frac{1}{M_B}\sigma a l\big(1-\bar{A}\big) + \bar{C}u_{1s}\end{aligned} \tag{30a}$$

$$\begin{aligned}\Omega_0 B(1+A) = {} & -\frac{1}{2I_B}\varepsilon a^2 n(1-A)V_0\tau_{n0} \\ & - \frac{1}{2I_B}\mu\gamma a^2\sigma l(1-A) + Cu_{2s}.\end{aligned} \tag{30b}$$

This condition also leads to a constant depth of cut d_0 and a constant delay τ_{n0} [nominal value for τ_n in (23) and (28)] satisfying

$$d_0 = \frac{2\pi V_0}{\Omega_0} \tag{31}$$

$$\tau_{n0} = \frac{2\pi}{n\Omega_0} \tag{32}$$

which are obtained by substituting (29) into (11) and (12), respectively.

In line with the model formulations in [14], [17], and [24], the following scaled perturbed quantities are introduced by using the characteristic time $t_* = c_t L$ and characteristic length $L_* = L$:

$$u = \frac{U_b - U_s}{L_*} \tag{33a}$$
$$\varphi = \theta_b - \theta_s \tag{33b}$$
$$r_1 = \bar{C} c_t^2 L (u_1 - u_{1s}) \tag{33c}$$
$$r_2 = C c_t^2 L^2 (u_2 - u_{2s}). \tag{33d}$$

Subsequently, the dimensionless perturbation dynamics is given by

$$\begin{aligned}
&u''(\hat{t}) - \bar{A}u''(\hat{t} - 2\hat{\tau}_a)\\
&\quad = -\bar{N}u'(\hat{t}) - \bar{A}\bar{N}u'(\hat{t} - 2\hat{\tau}_a) - \bar{\psi}\big(u(\hat{t}) - u(\hat{t} - \hat{\tau}_n(\hat{t}))\big)\\
&\qquad + \bar{\psi}\bar{A}\big(u(\hat{t} - 2\hat{\tau}_a) - u(\hat{t} - 2\hat{\tau}_a - \hat{\tau}_n(\hat{t} - 2\hat{\tau}_a))\big)\\
&\qquad - \bar{\psi}\nu_0\big(\hat{\tau}_n(\hat{t}) - \hat{\tau}_{n0}\big) + \bar{\psi}\bar{A}\nu_0\big(\hat{\tau}_n(\hat{t} - 2\hat{\tau}_a) - \hat{\tau}_{n0}\big)\\
&\qquad + r_1(\hat{t} - \hat{\tau}_a)
\end{aligned} \tag{34a}$$
$$\begin{aligned}
&\varphi''(\hat{t}) - A\varphi''(\hat{t} - 2\hat{\tau}_t)\\
&\quad = -N\varphi'(\hat{t}) - AN\varphi'(\hat{t} - 2\hat{\tau}_t) - \psi\big(u(\hat{t}) - u(\hat{t} - \hat{\tau}_n(\hat{t}))\big)\\
&\qquad + \psi A\big(u(\hat{t} - 2\hat{\tau}_t) - u(\hat{t} - 2\hat{\tau}_t - \hat{\tau}_n(\hat{t} - 2\hat{\tau}_t))\big)\\
&\qquad - \psi\nu_0\big(\hat{\tau}_n(\hat{t}) - \hat{\tau}_{n0}\big) + \psi A\nu_0\big(\hat{\tau}_n(\hat{t} - 2\hat{\tau}_t) - \hat{\tau}_{n0}\big)\\
&\qquad + r_2(\hat{t} - \hat{\tau}_t)
\end{aligned} \tag{34b}$$

where the scaled time and scaled time delays are defined as follows:

$$\hat{t} = \frac{t}{t_*}, \quad \hat{\tau}_a = \frac{\tau_a}{t_*}, \ \hat{\tau}_t = \frac{\tau_t}{t_*}, \ \hat{\tau}_{n0} = \frac{\tau_{n0}}{t_*} \tag{35}$$

and the dimensionless state-dependent delay $\hat{\tau}_n(t)$ in terms of the perturbation coordinates can be obtained from

$$\varphi(\hat{t}) - \varphi(\hat{t} - \hat{\tau}_n(\hat{t})) + \omega_0\hat{\tau}_n(\hat{t}) = \frac{2\pi}{n}. \tag{36}$$

Moreover, in (34) and (36), ω_0 and ν_0 are the scaled nominal velocities given by

$$\omega_0 = \Omega_0 t_*, \quad \nu_0 = c_t V_0. \tag{37}$$

Note that the prime $()'$ in (34) indicates differentiation with respect to the scaled time $\hat{t}$ and

$$\begin{aligned}
\bar{N} &= \bar{B}c_t L, \quad N = Bc_t L\\
\bar{\psi} &= \frac{1}{M_B}\varepsilon a\zeta n c_t^2 L^2, \quad \psi = \frac{1}{2I_B}\varepsilon a^2 n c_t^2 L^3.
\end{aligned} \tag{38}$$

Motivated by [24], (36) can be rewritten as

$$\hat{\tau}_n(\hat{t}) - \hat{\tau}_{n0} = -\frac{\varphi(\hat{t}) - \varphi(\hat{t} - \hat{\tau}_n(\hat{t}))}{\omega_0} \tag{39}$$

since $\hat{\tau}_{n0} = 2\pi/n\omega_0$. Substituting (39) into (34), the dimensionless perturbation dynamics can be rewritten as follows:

$$\begin{aligned}
&u''(\hat{t}) - \bar{A}u''(\hat{t} - 2\hat{\tau}_a)\\
&\quad = -\bar{N}u'(\hat{t}) - \bar{A}\bar{N}u'(\hat{t} - 2\hat{\tau}_a) - \bar{\psi}\big(u(\hat{t}) - u(\hat{t} - \hat{\tau}_n(\hat{t}))\big)\\
&\qquad + \bar{\psi}\bar{A}\big(u(\hat{t} - 2\hat{\tau}_a) - u(\hat{t} - 2\hat{\tau}_a - \hat{\tau}_n(\hat{t} - 2\hat{\tau}_a))\big)\\
&\qquad - \bar{Q}\big(\varphi(\hat{t}) - \varphi(\hat{t} - \hat{\tau}_n(\hat{t}))\big)\\
&\qquad + \bar{Q}\bar{A}\big(\varphi(\hat{t} - 2\hat{\tau}_a) - \varphi(\hat{t} - 2\hat{\tau}_a - \hat{\tau}_n(\hat{t} - 2\hat{\tau}_a))\big)\\
&\qquad + r_1(\hat{t} - \hat{\tau}_a)
\end{aligned} \tag{40a}$$
$$\begin{aligned}
&\varphi''(\hat{t}) - A\varphi''(\hat{t} - 2\hat{\tau}_t)\\
&\quad = -N\varphi'(\hat{t}) - AN\varphi'(\hat{t} - 2\hat{\tau}_t) - \psi\big(u(\hat{t}) - u(\hat{t} - \hat{\tau}_n(\hat{t}))\big)\\
&\qquad + \psi A\big(u(\hat{t} - 2\hat{\tau}_t) - u(\hat{t} - 2\hat{\tau}_t - \hat{\tau}_n(\hat{t} - 2\hat{\tau}_t))\big)\\
&\qquad - Q\big(\varphi(\hat{t}) - \varphi(\hat{t} - \hat{\tau}_n(\hat{t}))\big)\\
&\qquad + QA\big(\varphi(\hat{t} - 2\hat{\tau}_t) - \varphi(\hat{t} - 2\hat{\tau}_t - \hat{\tau}_n(\hat{t} - 2\hat{\tau}_t))\big)\\
&\qquad + r_2(\hat{t} - \hat{\tau}_t)
\end{aligned} \tag{40b}$$

where

$$\bar{Q} = -\bar{\psi}\delta_0/2\pi, \quad Q = -\psi\delta_0/2\pi \tag{41}$$

with δ_0 the dimensionless nominal depth of cut defined as

$$\delta_0 = \frac{d_0}{L_*} = \frac{2\pi\nu_0}{\omega_0}. \tag{42}$$

Note that (40) is preferred to (34) since the former equations do not depend explicitly on the state-dependent delay $\hat{\tau}_n$.

D. Associated Linearized System Dynamics

State-dependent delay differential equations (SD-DDEs), such as those in (40) with (36), are nonlinear as the state argument is a function of the state itself [55]. Therefore, by linearization, we mean obtaining an associated linear DDE with the same local stability features as the original nonlinear system.

The linearization of neutral-type SD-DDEs has been studied in [56], where it is shown that the exponential stability of the trivial solution of the associated linearized equation implies the exponential stability of a constant steady-state solution of the original NDDE.

Introducing the state vector $x^T = [x_1 \ \ x_2 \ \ x_3 \ \ x_4] := [u \ \ u' \ \ \varphi \ \ \varphi']$, (40) is rewritten as follows:

$$\begin{aligned}
&x'(\hat{t}) - E_1 x'(\hat{t} - \hat{\tau}_1) - E_2 x'(\hat{t} - \hat{\tau}_2)\\
&\quad = f\big(x(\hat{t}), x(\hat{t} - \hat{\tau}_1), x(\hat{t} - \hat{\tau}_2), x(\hat{t} - \hat{\tau}_3), x(\hat{t} - \hat{\tau}_4), x(\hat{t} - \hat{\tau}_5)\big)\\
&\qquad + B_1 r_1(\hat{t} - \hat{h}_1) + B_2 r_2(\hat{t} - \hat{h}_2)
\end{aligned} \tag{43}$$

where $f = [f_1 \ \ f_2 \ \ f_3 \ \ f_4]^T$ with

$$\begin{aligned}
f_1 &= x_2(\hat{t})\\
f_2 &= -\bar{N}x_2(\hat{t}) - \bar{A}\bar{N}x_2(\hat{t} - \hat{\tau}_1) - \bar{\psi}\big(x_1(\hat{t}) - x_1(\hat{t} - \hat{\tau}_3)\big)\\
&\quad + \bar{\psi}\bar{A}\big(x_1(\hat{t} - \hat{\tau}_1) - x_1(\hat{t} - \hat{\tau}_4)\big)\\
&\quad - \bar{Q}\big(x_3(\hat{t}) - x_3(\hat{t} - \hat{\tau}_3)\big)\\
&\quad + \bar{Q}\bar{A}\big(x_3(\hat{t} - \hat{\tau}_1) - x_3(\hat{t} - \hat{\tau}_4)\big)\\
f_3 &= \ \ x_4(\hat{t})\\
f_4 &= -Nx_4(\hat{t}) - ANx_4(\hat{t} - \hat{\tau}_2) - \psi\big(x_1(\hat{t}) - x_1(\hat{t} - \hat{\tau}_3)\big)\\
&\quad + \psi A\big(x_1(\hat{t} - \hat{\tau}_2) - x_1(\hat{t} - \hat{\tau}_5)\big)\\
&\quad - Q\big(x_3(\hat{t}) - x_3(\hat{t} - \hat{\tau}_3)\big)\\
&\quad + QA\big(x_3(\hat{t} - \hat{\tau}_2) - x_3(\hat{t} - \hat{\tau}_5)\big).
\end{aligned} \tag{44}$$

The matrices in (43) are defined as follows:

$$E_1 = \begin{bmatrix} 0 & 0 & 0 & 0 \\ 0 & \bar{A} & 0 & 0 \\ 0 & 0 & 0 & 0 \\ 0 & 0 & 0 & 0 \end{bmatrix}, \quad E_2 = \begin{bmatrix} 0 & 0 & 0 & 0 \\ 0 & 0 & 0 & 0 \\ 0 & 0 & 0 & 0 \\ 0 & 0 & 0 & A \end{bmatrix}$$
$$B_1 = \begin{bmatrix} 0 \\ 1 \\ 0 \\ 0 \end{bmatrix}, \quad B_2 = \begin{bmatrix} 0 \\ 0 \\ 0 \\ 1 \end{bmatrix} \tag{45}$$

and the time delays are given by

$$\begin{aligned} &\hat{\tau}_1 = 2\hat{\tau}_a, \quad \hat{\tau}_2 = 2\hat{\tau}_t, \ \ \hat{\tau}_3 = \hat{\tau}_n(x_t) \\ &\hat{\tau}_4 = 2\hat{\tau}_a + \hat{\tau}_n(x_t), \quad \hat{\tau}_5 = 2\hat{\tau}_t + \hat{\tau}_n(x_t) \\ &\hat{h}_1 = \hat{\tau}_a, \quad \hat{h}_2 = \hat{\tau}_t. \end{aligned} \tag{46}$$

The notation $\hat{\tau}_n(x_t)$ is simply indicating that $\hat{\tau}_n$ is a state-dependent delay, where x_t denotes the past function segment of the state variables, defined as $x_t(s) := x(t+s), \quad s \in [-\hat{\tau}_n, 0]$.

Based on [56], the linearized system associated with the constant solution $x(\hat{t}) = x_0 = [0 \quad 0 \quad 0 \quad 0]^T$ is given by

$$\begin{aligned} &x'(\hat{t}) - E_1 x'(\hat{t} - \bar{\tau}_1) - E_2 x'(\hat{t} - \bar{\tau}_2) \\ &= D_1 f(x_0, x_0, x_0, x_0, x_0, x_0) x(\hat{t}) \\ &\quad + \sum_{i=1}^{5} D_{i+1} f(x_0, x_0, x_0, x_0, x_0, x_0) x(\hat{t} - \bar{\tau}_i) \\ &\quad + B_1 r_1(\hat{t} - \bar{h}_1) + B_2 r_2(\hat{t} - \bar{h}_2) \end{aligned} \tag{47}$$

where

$$\begin{aligned} &\bar{\tau}_1 = \hat{\tau}_1, \quad \bar{\tau}_2 = \hat{\tau}_2, \ \ \bar{\tau}_3 = \hat{\tau}_n(x_0) \\ &\bar{\tau}_4 = 2\hat{\tau}_a + \hat{\tau}_n(x_0), \quad \bar{\tau}_5 = 2\hat{\tau}_t + \hat{\tau}_n(x_0) \\ &\bar{h}_1 = \hat{h}_1, \quad \bar{h}_2 = \hat{h}_2. \end{aligned} \tag{48}$$

The constant delay $\hat{\tau}_n(x_0)$ is obtained by substitution of $x(\hat{t}) \equiv x_0$ in (36), which results in $\hat{\tau}_n(x_0) = 2\pi/n\omega_0$. Note that $D_i f$ in (47) indicates the derivatives of f with respect to the ith argument of f. Finally, the linearized nondimensional perturbation dynamics can be written in the following form:

$$x'(\hat{t}) - \sum_{i=1}^{2} E_i x'(\hat{t} - \bar{\tau}_i) = A_0 x(\hat{t}) + \sum_{i=1}^{5} A_i x(\hat{t} - \bar{\tau}_i) + \sum_{i=1}^{2} B_i r_i(\hat{t} - \bar{h}_i) \tag{49}$$

where $A_i := D_{i+1} f(x_0, x_0, x_0, x_0, x_0, x_0)$ gives

$$A_0 = \begin{bmatrix} 0 & 1 & 0 & 0 \\ -\bar{\psi} & -\bar{N} & -\bar{Q} & 0 \\ 0 & 0 & 0 & 1 \\ -\psi & 0 & -Q & -N \end{bmatrix}$$
$$A_1 = \begin{bmatrix} 0 & 0 & 0 & 0 \\ \bar{\psi}\bar{A} & -\bar{A}\bar{N} & \bar{Q}\bar{A} & 0 \\ 0 & 0 & 0 & 0 \\ 0 & 0 & 0 & 0 \end{bmatrix}$$
$$A_2 = \begin{bmatrix} 0 & 0 & 0 & 0 \\ 0 & 0 & 0 & 0 \\ 0 & 0 & 0 & 0 \\ \psi A & 0 & QA & -AN \end{bmatrix}$$
$$A_3 = \begin{bmatrix} 0 & 0 & 0 & 0 \\ \bar{\psi} & 0 & \bar{Q} & 0 \\ 0 & 0 & 0 & 0 \\ \psi & 0 & Q & 0 \end{bmatrix}$$
$$A_4 = \begin{bmatrix} 0 & 0 & 0 & 0 \\ -\bar{\psi}\bar{A} & 0 & -\bar{Q}\bar{A} & 0 \\ 0 & 0 & 0 & 0 \\ 0 & 0 & 0 & 0 \end{bmatrix}$$
$$A_5 = \begin{bmatrix} 0 & 0 & 0 & 0 \\ 0 & 0 & 0 & 0 \\ 0 & 0 & 0 & 0 \\ -\psi A & 0 & -QA & 0 \end{bmatrix}. \tag{50}$$

Summarizing, in this section, the associated linearized perturbation dynamics has been obtained. These dynamics [see (49)] are formulated in terms of NDDEs with constant state delays and constant input delays. The latter is important in the context of control since it supports the application of the continuous pole-placement method [48] for controller synthesis, which is applicable on linear time-invariant time-delay systems.

III. Control Problem Formulation

In the drilling industry, it is desired to realize constant axial and angular velocities during operation. Therefore, we design a state-feedback control law that drives the downhole velocities, $\dot{U}_b(t)$ and $\dot{\theta}_b(t)$, to constant (and positive) set-point values V_0 and Ω_0, respectively. Note that this is achieved if the equilibrium $x = 0$ of (49) is stabilized. Toward this goal, we employ two control inputs, the dimensionless force $r_1(\hat{t})$ and the dimensionless torque $r_2(\hat{t})$, which enter the dynamics in a delayed fashion [see (49)].

For drilling systems, there are different methods of data transmission from well-bottom to the top (mud-pulse telemetry, acoustic waves, and so on). These downhole sensing methods introduce significant time delays and are subjected to significant noise levels. Besides, the downhole sensors are prone to failure due to harsh downhole conditions. Therefore, in this article, we only employ the top-side measurements, i.e., the rate of penetration and angular velocity measured at the top-drive $[(\partial U_{\text{top}})/(\partial t)$ and $(\partial \theta_{\text{top}})/(\partial t)$, respectively] and the data concerning the saver sub force and saver sub torque $[(\partial U_{\text{top}})/(\partial s)$ and $(\partial \theta_{\text{top}})/(\partial s)$, respectively]. Consequently, $(\partial U_b)/(\partial t)(t-\tau_a)$ and $(\partial \theta_b)/(\partial t)(t-\tau_t)$ are available (indirectly) due to the use of relations (3a) and (3b), respectively. Subsequently, the dimension-less measured output vector $y(\hat{t})^T = [y_1 \quad y_2] := [u'(\hat{t} - \hat{\tau}_a) \quad \varphi'(\hat{t} - \hat{\tau}_t)]$ is expressed as follows:

$$y(\hat{t}) = C_1 x(\hat{t} - \hat{\tau}_a) + C_2 x(\hat{t} - \hat{\tau}_t) \tag{51}$$

where

$$C_1 = \begin{bmatrix} 0 & 1 & 0 & 0 \\ 0 & 0 & 0 & 0 \end{bmatrix}, \quad C_2 = \begin{bmatrix} 0 & 0 & 0 & 0 \\ 0 & 0 & 0 & 1 \end{bmatrix}. \tag{52}$$

Note that $u'(\hat{t} - \hat{\tau}_D)$ and $\varphi'(\hat{t} - \hat{\tau}_D)$ are also available for any given $\hat{\tau}_D \geq \max(\hat{\tau}_a, \hat{\tau}_t)$.

The main controller goal is to stabilize the linearized dimensionless perturbation dynamics (49) by only using the available measurements (the output $y(\hat{t})$ (51) and its delayed versions). To facilitate controller synthesis, the spectrum of the open-loop system is analyzed in Section IV, which supports the stability analysis and the assessment of stabilizability properties. The controller design is pursued in Section V, under the premise of stabilizability.

IV. Stability Analysis and Stabilizability

In this section, a spectral approach [57] is employed to analyze the stability of the presented linearized drilling dynamics to study the root causes for drill-string vibrations and to serve as a basis for controller design. Although the eigenvalue-based framework presented in [57] is developed for a class of DDEs called delay differential-algebraic equations (DDAEs), NDDEs, such as those in (49), can also be analyzed in this framework.

By introducing a new state vector $X(\hat{t}) = [z(\hat{t}) \quad x(\hat{t})]^T$, where the variable $z(\hat{t})$ is expressed as

$$z(\hat{t}) = x(\hat{t}) - \sum_{i=1}^{2} E_i x(\hat{t} - \bar{\tau}_i). \tag{53}$$

Equation (49) can be reformulated as a DDAE as follows:

$$\mathfrak{E}_0 \; X'(\hat{t}) = \mathfrak{A}_0 \; X(\hat{t}) + \sum_{i=1}^{5} \mathfrak{A}_i X(\hat{t} - \bar{\tau}_i) + \sum_{i=1}^{2} \mathfrak{B}_i r_i(\hat{t} - \bar{h}_i) \tag{54}$$

where the matrices are defined as follows:

$$\mathfrak{E}_0 = \begin{bmatrix} I & 0 \\ 0 & 0 \end{bmatrix}, \quad \mathfrak{A}_0 = \begin{bmatrix} 0 & A_0 \\ -I & I \end{bmatrix}$$
$$\mathfrak{A}_i = \begin{cases} \begin{bmatrix} 0 & A_i \\ 0 & -E_i \end{bmatrix}, & \text{for } i = 1, 2 \\ \begin{bmatrix} 0 & A_i \\ 0 & 0 \end{bmatrix}, & \text{otherwise} \end{cases} \qquad \mathfrak{B}_i = \begin{bmatrix} B_i \\ 0 \end{bmatrix}, \; i = 1, 2. \tag{55}$$

The inverse transformation (from DDAE to NDDE) can take place by differentiating the variable in (53). The equivalence of the spectrum of an NDDE and its corresponding DDAE depends on how one transforms from one description to the other. When this operation involves differentiation of an equation, additional dynamics is introduced, which is reflected by additional characteristic roots at zero. However, one can always transform an NDDE to DDAE, without introducing any additional characteristic root. Hence, the analysis can be done based on the NDDEs and the transformation to DDAEs is performed whenever it is needed (e.g., when using TDS-STABIL [58] MATLAB package to find the stability-relevant characteristic roots).

A. Stability Analysis

The equilibrium $x = 0$ of (49) [or $X = 0$ for the equivalent formulation (54)] is exponentially stable if and only if all the characteristic roots are located in the left-half complex plane (LHP) and away from the imaginary axis [59].

A retarded-type delay differential equation (RDDE) always has a finite number of characteristic roots in the right-half complex plane (RHP), whereas an NDDE may have an infinite number of characteristic roots in the RHP or on the imaginary axis [59]. Such properties can effectively be analyzed using Proposition 1 below. In support of Proposition 1, the spectral abscissa of the delay difference equation associated with (49) and defined as follows:

$$x(\hat{t}) - \sum_{i=1}^{2} E_i x(\hat{t} - \bar{\tau}_i) = 0 \tag{56}$$

is expressed as

$$c_D := \sup\{\mathrm{Re}(\lambda) : \det \Delta_D(\lambda) = 0\} \tag{57}$$

where $\Delta_D(\lambda)$ is the characteristic matrix of the delay difference equation, which is given by

$$\Delta_D(\lambda) := I - \sum_{i=1}^{2} E_i e^{-\lambda \bar{\tau}_i} = \begin{bmatrix} 1 & 0 & 0 & 0 \\ 0 & 1 - \bar{A} e^{-\lambda \bar{\tau}_1} & 0 & 0 \\ 0 & 0 & 1 & 0 \\ 0 & 0 & 0 & 1 - A e^{-\lambda \bar{\tau}_2} \end{bmatrix}. \tag{58}$$

Proposition 1: [57] There exists a sequence $\{\lambda_k\}_{k \geq 1}$ of characteristic roots satisfying

$$\lim_{k \to \infty} \mathrm{Re}(\lambda_k) = c_D, \quad \lim_{k \to \infty} \mathrm{Im}(\lambda_k) = \infty. \tag{59}$$

Remark 1: We observe that not only there exists a sequence of characteristic roots with real parts converging to c_D and imaginary parts tending to infinity (see Proposition 1), but also there exists such sequences for each member of the set $\mathbf{C}_D = \{\mathrm{Re}(\lambda) : \det \Delta_D(\lambda) = 0\}$. Clearly, given (57), the one mentioned in Proposition 1 is the right-most one.

Therefore, if $c_D < 0$, all such sequences of characteristic roots are located in the LHP, which ensures that only a finite number of characteristic roots can potentially lie in the RHP. This feature plays an important role in the analysis of stabilizability of the system as pursued in Section IV-B.

B. Stabilizability

An NTD system is exponentially stabilizable by state feedback if and only if it is "formally stable" and "spectrally stabilizable" [47]. A system is called "formally stable" if it has at most a finite number of characteristic roots in the RHP, i.e., if $c_D < 0$. The importance of the formal stability property in the scope of the existence of a stabilizing state-feedback controller can be understood as follows. Since a state-feedback controller does not affect the delay difference equation in (56), an open-loop system that is not formally stable leads to an infinite number of unstable characteristic roots in the closed-loop system. Note that the input transformation (8) was introduced to render the system formally stable.

The property of "spectral stabilizability" of the system can be investigated using the following proposition.

Proposition 2: [47] An NTD system of the form

$$\dot{q}(t) - \sum_{i=1}^{F} \mathbb{E}_i \dot{q}(t-\tau_i) = \sum_{i=1}^{F} \mathbb{A}_i q(t-\tau_i) + \sum_{i=1}^{F} \mathbb{B}_i u(t-\tau_i) \tag{60}$$

with the state vector $q(t) \in \mathbb{R}^n$, input vector $u(t) \in \mathbb{R}^m$, and time delays

$$0 < \tau_1 < \tau_2 < \cdots < \tau_F$$

is spectrally stabilizable if

$$\operatorname{rank}\big[\lambda\big(I - \hat{\mathbb{E}}(\lambda)\big) - \hat{\mathbb{A}}(\lambda), \quad \hat{\mathbb{B}}(\lambda)\big] = n \quad \forall\lambda|\mathrm{Re}(\lambda) \geq 0 \tag{61}$$

where

$$\hat{\mathbb{E}} = \sum_{i=1}^{F} \mathbb{E}_i e^{-\lambda\tau_i}, \quad \hat{\mathbb{A}} = \sum_{i=1}^{F} \mathbb{A}_i e^{-\lambda\tau_i}, \ \hat{\mathbb{B}} = \sum_{i=1}^{F} \mathbb{B}_i e^{-\lambda\tau_i}. \tag{62}$$

For a system of the form (60) that is "formally stable" and "spectrally stabilizable," the stabilizability is assured by a state-feedback control law of the following form [60]:

$$u(t) = -\sum_{i=1}^{H} K_i q(t-\alpha_i) \tag{63}$$

where K_i are the gain matrices and

$$\alpha_i = \sum_{j=1}^{F} m_{ij}\tau_j, \quad i = 1, \ldots, H, \ m_{ij} \in \mathbb{Z}, \ H \in \mathbb{N}. \tag{64}$$

For the system under study, the spectral stabilizabilty can be analyzed, using the rank condition given in (61) with the following matrices:

$$\hat{\mathbb{E}} = \sum_{i=1}^{2} E_i e^{-\lambda\bar{\tau}_i}, \quad \hat{\mathbb{A}} = A_0 + \sum_{i=1}^{5} A_i e^{-\lambda\bar{\tau}_i}, \ \hat{\mathbb{B}} = \sum_{i=1}^{2} B_i e^{-\lambda\bar{h}_i}. \tag{65}$$

A quantitative stability analysis and analysis of stabilizability are pursued for an exemplary drill-string system in Section VII. Under the premise of stabilizability, we pursue the design of a stabilizing state-feedback controller in Section V.

V. Controller Design Methodology

In this section, the continuous pole-placement approach [48] is employed to design a state-feedback controller, aiming at stabilizing (49) and (50). In particular, the objective of this state-feedback controller is to place all roots in the LHP, which, in turn, results in an asymptotically stable closed-loop system.

The state-feedback control law is designed as follows to compensate for the input delays in (49):

$$\begin{aligned} r_1(\hat{t}) &= K_{11}x(\hat{t}+\bar{h}_1) + K_{12}x(\hat{t}-\bar{\tau}_1+\bar{h}_1) \\ &\quad + K_{13}x(\hat{t}-\bar{\tau}_3+\bar{h}_1) \end{aligned} \tag{66a}$$

$$\begin{aligned} r_2(\hat{t}) &= K_{21}x(\hat{t}+\bar{h}_2) + K_{22}x(\hat{t}-\bar{\tau}_2+\bar{h}_2) \\ &\quad + K_{23}x(\hat{t}-\bar{\tau}_3+\bar{h}_2) \end{aligned} \tag{66b}$$

with K_{ij}, $i \in \{1, 2\}$ and $j \in \{1, 2, 3\}$, the gain matrices. Note that in the proposed control law (66), both the axial and torsional inputs, r_1 and r_2, are influenced by the related axial and torsional time delays (or axial and torsional wave speeds), respectively. Subsequently, the closed-loop tracking error dynamics is given by

$$x'(\hat{t}) - \sum_{i=1}^{2} E_i x'(\hat{t}-\bar{\tau}_i) = \mathscr{A}_0 \, x(\hat{t}) + \sum_{i=1}^{5} \mathscr{A}_i x(\hat{t}-\bar{\tau}_i) \tag{67}$$

where

$$\begin{aligned} &\mathscr{A}_0 = A_0 + B_1 \ K_{11} + B_2 \ K_{21}, \quad \mathscr{A}_1 = A_1 + B_1 \ K_{12} \\ &\mathscr{A}_2 = A_2 + B_2 \ K_{22}, \quad \mathscr{A}_3 = A_3 + B_1 \ K_{13} + B_2 \ K_{23} \\ &\mathscr{A}_4 = A_4, \quad \mathscr{A}_5 = A_5. \end{aligned} \tag{68}$$

The following structure is imposed on the gain matrices K_{ij} to, first, alleviate the computational burden of the optimization-based tuning of these gains and, second, avoid using delayed downhole angular and axial positions that are not available by measurement (note that there is no sensor at the bit that measures the bit position):

$$\begin{aligned} &K_{11} = [\,k_1 \quad k_2 \quad k_3 \quad 0\,], \quad K_{21} = [\,k_7 \quad 0 \quad k_8 \quad k_9\,] \\ &K_{12} = [\,0 \quad k_4 \quad 0 \quad 0\,], \quad K_{22} = [\,0 \quad 0 \quad 0 \quad k_{10}\,] \\ &K_{13} = [\,k_5 \quad 0 \quad k_6 \quad 0\,], \quad K_{23} = [\,k_{11} \quad 0 \quad k_{12} \quad 0\,] \end{aligned} \tag{69}$$

where k_i, $i = 1, \ldots, 12$, represent the nonzero gain elements. With these gain matrices, the state-feedback control law (66) can be written explicitly as follows:

$$\begin{aligned} r_1(\hat{t}) &= k_1 u(\hat{t}+\bar{h}_1) + k_2 u'(\hat{t}+\bar{h}_1) + k_3\varphi(\hat{t}+\bar{h}_1) \\ &\quad + k_4 u'(\hat{t}-\bar{\tau}_1+\bar{h}_1) \\ &\quad + k_5 u(\hat{t}-\bar{\tau}_3+\bar{h}_1) + k_6\varphi(\hat{t}-\bar{\tau}_3+\bar{h}_1) \end{aligned} \tag{70a}$$

$$\begin{aligned} r_2(\hat{t}) &= k_7 u(\hat{t}+\bar{h}_2) + k_8\varphi(\hat{t}+\bar{h}_2) + k_9\varphi'(\hat{t}+\bar{h}_2) \\ &\quad + k_{10}\varphi'(\hat{t}-\bar{\tau}_2+\bar{h}_2) \\ &\quad + k_{11} u(\hat{t}-\bar{\tau}_3+\bar{h}_2) + k_{12}\varphi(\hat{t}-\bar{\tau}_3+\bar{h}_2). \end{aligned} \tag{70b}$$

In (70), the terms with the argument $\hat{t}+\bar{h}_1$ and $\hat{t}+\bar{h}_2$ are future states since $\bar{h}_1, \bar{h}_2 > 0$. The terms with the argument $\hat{t}-\bar{\tau}_3+\bar{h}_1$ and $\hat{t}-\bar{\tau}_3+\bar{h}_2$ are also future states because $\bar{\tau}_3$, i.e., the delay induced by the cutting process at the bit, is smaller than $\bar{h}_1$ and $\bar{h}_2$, i.e., the delays induced by the axial and torsional wave propagation in the drill string. These terms render the control law noncausal. To arrive at a causal implementation, this control law will be combined with a predictor, which will be proposed in Section VI. Moreover, there are two other delayed terms in (70), $u'(\hat{t}-\bar{\tau}_1+\bar{h}_1)$ and $\varphi'(\hat{t}-\bar{\tau}_2+\bar{h}_2)$ (i.e., $u'(\hat{t}-\hat{\tau}_a)$ and $\varphi'(\hat{t}-\hat{\tau}_t)$, respectively), which are available by top-side measurements, as discussed in Section III.

Next, we design the control gains k_i in (69) by an optimization method for pole placement. The underlying optimization problem is considered as a procedure of finding controller gains for which the spectral abscissa (i.e., the real part of the right-most characteristic root) of the closed-loop system is strictly negative. Hence, the objective function is formulated as follows:

$$F(k_i) = \sup\{\mathrm{Re}(\lambda) : \det \Delta_N(\lambda) = 0\} \tag{71}$$

where $\Delta_N(\lambda)$ is the characteristic matrix of the closed-loop system (67), which is which is founded defined as follows:

$$\Delta_N(\lambda) := \lambda\left(I - \sum_{i=1}^{2} E_i e^{-\lambda\bar{\tau}_i}\right) - \mathscr{A}_0 - \sum_{i=1}^{5} \mathscr{A}_i e^{-\lambda\bar{\tau}_i}. \tag{72}$$

Asymptotic stability is guaranteed when the objective function (71) is negative. In particular, the continuous pole-placement method aims at designing k_i such that the optimization problem $\min_{k_i} F(k_i)$ is solved with the stopping criterion $F(k_i) \le \delta$ for a given $\delta < 0$.

Since the objective function in (71) is a nonsmooth function of the controller parameters, common optimization algorithms are not applicable [59]. Instead, the HANSO[1] method [61] has been employed, which is founded on the BFGS[2] and gradient sampling methods [62]. It is noteworthy to mention that in this article, the PSO[3] [63] method has been used in order to search globally for a proper initial guess of the controller gains in order to avoid convergence to local minima.

VI. Predictor Design Methodology

The designed feedback controller in (70), presented in Section V, is noncausal as it requires the knowledge of future states. To make such controller causal, the use of a proper predictor is essential. The predictor design for linear time-delay systems has been taken into consideration in the series of studies [64]–[68] for systems, including different combinations of state delays, (one or several) input delays, and neutral terms. However, the implementation of such ideas includes approximating some integral terms, which makes the closed-loop system unstable, since the approximation introduces new unstable eigenvalues. The implementation complexity is explained thoroughly in [69] and [70], where the design of a low-pass filter is suggested to overcome such a problem. Another approach proposes to estimate the future states in an asymptotic way, instead of approximation, by using an observer-like structure (see [71]–[73]).

Here, based on the work in [71]–[73], a predictor with an observer-like structure is presented to estimate the future states asymptotically. The formulation presented in [71]–[73] can be applied directly to systems that, first, have a single input and, second, the prediction time is equal to the input delay. However, the main underlying idea adapted to be applicable to systems with several inputs and including state delays (which may make the prediction time a combination of state delays and input delays, like those in this article).

[1]Hybrid algorithm for nonsmooth optimization.

[2]Broyden–Fletcher–Goldfarb–Shanno.

[3]Particle swarm optimization.

Based on the closed-loop system dynamics in (67), the predictor is designed as follows:

$$\begin{aligned}\omega'(\hat{t}) - \sum_{i=1}^{2} E_i \omega'(\hat{t} - \bar{\tau}_i) &= \mathscr{A}_0 \omega(\hat{t}) + \sum_{i=1}^{5} \mathscr{A}_i \omega(\hat{t} - \bar{\tau}_i) \\ &\quad - P\big(\omega(\hat{t} - \hat{\tau}_p - \hat{\tau}_m) - x(\hat{t} - \hat{\tau}_m)\big)\end{aligned} \tag{73}$$

where $\omega(\hat{t})$ is the estimate of the future states $x(\hat{t} + \hat{\tau}_p)$ for any given dimensionless time $\hat{\tau}_p$ with $\hat{\tau}_m = \max(\hat{\tau}_a, \hat{\tau}_t)$. As discussed in Section III, only delayed downhole velocities are available (by using top-side measurements). Thus, the following structure is considered for the predictor gain matrix P (in order to avoid using delayed downhole position measurements that are not available in practice):

$$P = \begin{bmatrix} 0 & p_1 & 0 & 0 \\ 0 & p_2 & 0 & 0 \\ 0 & 0 & 0 & p_3 \\ 0 & 0 & 0 & p_4 \end{bmatrix} \tag{74}$$

where p_i, $i = 1, \ldots, 4$, are the nonzero elements. Intuitively speaking, in (73) with the gain matrix (74), $x(\hat{t} + \hat{\tau}_p)$ is estimated by $\omega(\hat{t})$ by using $x_2(\hat{t} - \hat{\tau}_m)$ and $x_4(\hat{t} - \hat{\tau}_m)$ (i.e., $u'(\hat{t} - \hat{\tau}_m)$ and $\varphi'(\hat{t} - \hat{\tau}_m)$, respectively), which are both available at time $\hat{t}$ (see Section III).

Introducing the prediction error

$$e(\hat{t}) = \omega(\hat{t}) - x(\hat{t} + \hat{\tau}_p) \tag{75}$$

the prediction error dynamics is given by

$$\begin{aligned}e'(\hat{t}) - \sum_{i=1}^{2} E_i e'(\hat{t} - \bar{\tau}_i) &= \mathscr{A}_0\, e(\hat{t}) + \sum_{i=1}^{5} \mathscr{A}_i e(\hat{t} - \bar{\tau}_i) \\ &\quad - P e(\hat{t} - \hat{\tau}_p - \hat{\tau}_m).\end{aligned} \tag{76}$$

By design of the predictor gain matrix P, the equilibrium solution $e = 0$ of (76) can be rendered an asymptotically stable solution of (76), which implies the asymptotic convergence of $\omega(\hat{t})$ to $x(\hat{t} + \hat{\tau}_p)$.

The predictor gains p_i in (74) can be designed by an optimization-based method for pole placement. The underlying optimization problem is considered as a procedure of finding predictor gains for which the spectral abscissa of the prediction error dynamics is strictly negative. Hence, the objective function is formulated as follows:

$$F_P(p_i) = \sup\{\mathrm{Re}(\lambda) : \det \Delta_P(\lambda) = 0\} \tag{77}$$

where $\Delta_P(\lambda)$ is the characteristic matrix of the prediction error dynamics (76), which is defined as follows:

$$\begin{aligned}\Delta_P(\lambda) := \lambda\left(I - \sum_{i=1}^{2} E_i e^{-\lambda\bar{\tau}_i}\right) - \mathscr{A}_0 \\ - \sum_{i=1}^{5} \mathscr{A}_i e^{-\lambda\bar{\tau}_i} + P e^{-\lambda(\hat{\tau}_p + \hat{\tau}_m)}.\end{aligned} \tag{78}$$

Asymptotic stability is guaranteed when the objective function (77) is negative. In particular, the continuous pole-placement method aims at designing p_i such that the optimization

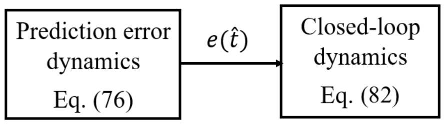

Fig. 2. Series connection of the prediction error dynamics and the closed-loop dynamics.

problem $\min_{p_i} F_P(p_i)$ is solved with the stopping criterion $F_P(p_i) \leq \delta$ for a given $\delta < 0$.

Remark 2: Note that even for $P = 0$, (76) is asymptotically stable. Hence, the design of P is geared toward rendering the error dynamics in (76) faster than those in (67).

For nonzero prediction error, the state-feedback control law (66) is given by

$$r_1(\hat{t}) = K_{01}\omega_1(\hat{t}) + K_{11}x(\hat{t} - \bar{\tau}_1 + \bar{h}_1) + K_{31}\omega_2(\hat{t}) \quad (79a)$$
$$r_2(\hat{t}) = K_{02}\omega_3(\hat{t}) + K_{22}x(\hat{t} - \bar{\tau}_2 + \bar{h}_2) + K_{32}\omega_4(\hat{t}) \quad (79b)$$

where $\omega_i(\hat{t})$, $i = 1, \ldots, 4$, are the estimates of the states $x(\hat{t} + \hat{\tau}_{pi})$ with prediction times

$$\hat{\tau}_{p1} = \bar{h}_1, \quad \hat{\tau}_{p2} = \bar{h}_1 - \bar{\tau}_3$$
$$\hat{\tau}_{p3} = \bar{h}_2, \quad \hat{\tau}_{p4} = \bar{h}_2 - \bar{\tau}_3. \quad (80)$$

Given (75), (79) can be written as follows:

$$\begin{aligned} r_1(\hat{t}) &= K_{01}x(\hat{t} + \bar{h}_1) + K_{11}x(\hat{t} - \bar{\tau}_1 + \bar{h}_1) \\ &\quad + K_{31}x(\hat{t} - \bar{\tau}_3 + \bar{h}_1) + K_{01}e_1(\hat{t}) + K_{31}e_2(\hat{t}) \quad (81a) \\ r_2(\hat{t}) &= K_{02}x(\hat{t} + \bar{h}_2) + K_{22}x(\hat{t} - \bar{\tau}_2 + \bar{h}_2) \\ &\quad + K_{32}x(\hat{t} - \bar{\tau}_3 + \bar{h}_2) + K_{02}e_3(\hat{t}) + K_{32}e_4(\hat{t}) \quad (81b) \end{aligned}$$

where e_i, $i = 1, \ldots, 4$, are the prediction errors at times $\hat{t}+\hat{\tau}_{pi}$. Subsequently, the closed-loop dynamics is given by

$$\begin{aligned} &x'(\hat{t}) - \sum_{i=1}^{2} E_i x'(\hat{t} - \bar{\tau}_i) \\ &= \mathscr{A}_0\, x(\hat{t}) + \sum_{i=1}^{5} \mathscr{A}_i x(\hat{t} - \bar{\tau}_i) \\ &\quad + B_1 K_{01} e_1(\hat{t} - \bar{h}_1) + B_1 K_{31} e_2(\hat{t} - \bar{h}_1) \\ &\quad + B_2 K_{02} e_3(\hat{t} - \bar{h}_2) + B_2 K_{32} e_4(\hat{t} - \bar{h}_2) \quad (82) \end{aligned}$$

which is the dynamics in (67) with additional input terms related to the prediction errors.

The following proposition states the conditions under which the proposed predictor-based control strategy indeed stabilizes the closed-loop system dynamics.

Proposition 3: Consider the drill-string dynamics in (49), (50). Let the controller in (79) be designed such that $F(k_i) < 0$, with $F(k_i)$ given in (71). Moreover, let the predictor in (73) be designed such that $F_P(p_i) < 0$, with $F_P(p_i)$ defined in (77). Then, the closed-loop dynamics (76) and (82) is asymptotically stable.

Proof: First, $F_P(p_i) < 0$ implies that the prediction error dynamics (76) is asymptotically stable. Second, $F(k_i) < 0$ implies that error dynamics in (67) (for zero prediction error) is asymptotically stable. By the grace of linearity of (82) and the fact that (82) is asymptotically stable for $e = 0$, it holds that (82) is input-to-state stable with the prediction error e as an input. Therefore, the total closed-loop dynamics is asymptotically stable based on the fact that it consists of a series connection of the asymptotically stable dynamics in (76) and the input-to-state stable dynamics in (82) (see Fig. 2). ■

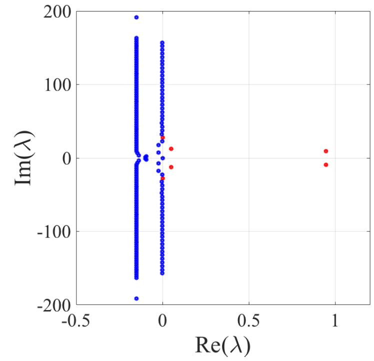

Fig. 3. Open-loop spectrum.

VII. Illustrative Simulation Results

In this section, we present a representative case study to illustratively show the effectiveness of the proposed control approach. In Section VII-A, the characteristics of the open-loop dynamics are investigated (stability and stabilizability properties), and in Section VII-B, the controller design is performed and the resulting closed-loop performance is analyzed.

A. Analysis of the Open-Loop Dynamics

For a 117-m long-drill-string with the parameter values given in Table I, the TDS-STABIL MATLAB package [58] is employed to find the stability-relevant characteristic roots of the infinite-dimensional model in (49) for $r_1 = r_2 = 0$, using (54) and (55). The open-loop spectrum is shown in Fig. 3, which illustrates that the system is intrinsically unstable since there are some characteristic roots in the RHP, depicted in red. Similar results have been obtained in the literature (see [14], [17], [20], [25] for lumped-parameter models and [5], [26] for infinite-dimensional models), which show that for realistic parametric settings, the nominal solution is generally unstable.

The behavior of the system (21) and (26) with the nonlinear bit–rock interaction law (10) is shown in Fig. 4 when constant control inputs, $u_1 = 16 \times 10^3$ N and $u_2 = 18 \times 10^3$ N·m, are employed. As shown, in the absence of any controller, severe stick-slip and bit-bouncing occur, which can lead to system failure.

As explained in Section IV, it is essential to investigate the exact place (i.e., real value) of the right-most vertical asymptote of the spectrum, as shown in Fig. 3. The spectral abscissa of the delay difference equation, given in (56), is $c_D \simeq -0.0022$, which shows that the asymptote is located in the LHP (see Proposition 1). The other asymptote, visible in Fig. 3, is located on -0.1510, which is the other root

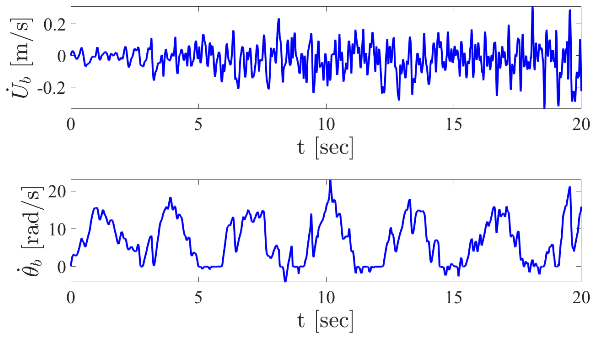

Fig. 4. Open-loop dynamics.

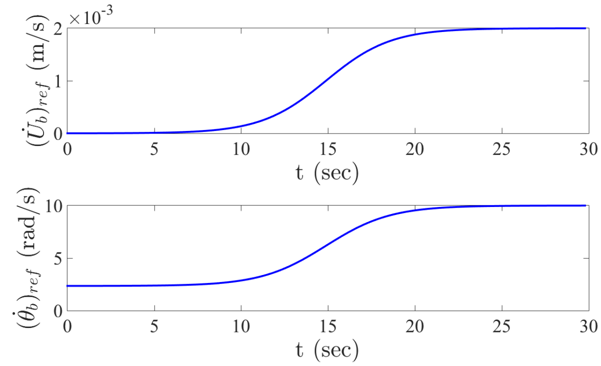

Fig. 5. Velocity references.

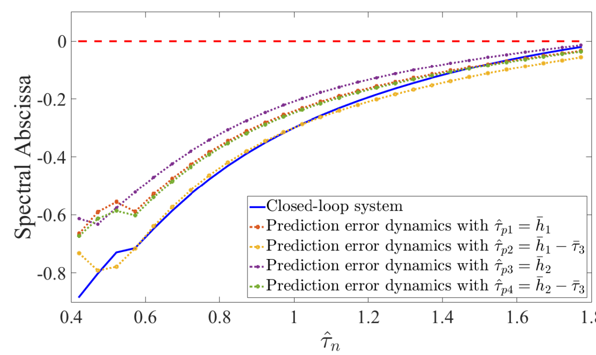

Fig. 6. Variation of spectral abscissa for different time delays $\hat{\tau}_n$. Note that $\hat{\tau}_n \in [0.4220, 1.7956]$ for $(\dot{\theta}_b)_{\text{ref}} \in [2.35, 10]$.

of $\det \Delta_D(\lambda) = 0$ (see Remark 1). Now, we can conclude that, first, there is only a finite number of characteristic roots in the RHP and, second, the roots are not accumulated on the imaginary axis. Therefore, the system is formally stable [47]. It is worth restating that the formal stability property is achieved as a result of the input transformation (8). Moreover, the spectral stabilizability of the system can be investigated based on Proposition 2. Since for all six characteristic roots with positive real parts (see red dots in Fig. 3), the rank condition in (61) holds, and it can be concluded that the system is indeed spectrally stabilizable. Therefore, the stabilizability of the presented drilling system (49) is assured by delayed state feedbacks of the form given in (63).

B. Controller Design and Closed-Loop Performance Analysis

The design procedure of the state-feedback controller, aiming at stabilizing (49), has been presented in Section V. In the following simulation study, we introduce the following smoothened references to deal with the actuator limitations (in particular, high-frequency content and large overshoots in the control inputs should be avoided in practice):

$$\left(\dot{U}_b\right)_{\text{ref}} = V_0 \frac{\exp(0.5373t - 8)}{1 + \exp(0.5373t - 8)} \tag{83a}$$

$$\left(\dot{\theta}_b\right)_{\text{ref}} = (\Omega_0 - 2.35)\frac{\exp(0.5373t - 8)}{1 + \exp(0.5373t - 8)} + 2.35. \tag{83b}$$

Introducing such reference design has also been suggested earlier in [28] and [33]. As shown in Fig. 5, the drill string has been first accelerated to a constant angular velocity, i.e., $(\dot{\theta}_b)_{\text{ref}}(t = 0) = 2.35$ rad/s, with the bit off bottom, i.e., $(\dot{U}_b)_{\text{ref}}(t = 0) = 0$ m/s. Then, both the axial and angular velocities are increased simultaneously to the desired operating conditions ($V_0 = 0.002$ m/s and $\Omega_0 = 10$ rad/s, respectively).

Remark 3: Although the references are time-varying, this does not disqualify the control design methodology presented in Section V, which was designed for linear time-invariant error dynamics, based on the following facts.

1) The system matrices of the error dynamics for time-varying reference remain time-invariant as these are not affected by the nominal solution.
2) Although the state-dependent delay $\hat{\tau}_n$ is time-varying along the time-varying angular reference trajectory in (83b), it can be shown that for any (constant) delay $\hat{\tau}_n$ induced by the angular velocities in the reference, the spectral abscissas of both the closed-loop dynamics and prediction error dynamics are always negative (see Fig. 6).
3) The reference (and hence also the state-dependent delay along the nominal solution) evolves on a much slower time scale than the dominant dynamics of the drill-string system.

Therefore, the control design methodology presented in V is extended as follows. With $x_{\text{ref}}(\hat{t}) := [u_{\text{ref}}(\hat{t})\ u'_{\text{ref}}(\hat{t})\ \varphi_{\text{ref}}(\hat{t})\ \varphi'_{\text{ref}}(\hat{t})]$ the desired reference trajectory, the tracking error $\tilde{x} := [\tilde{u}\ \tilde{u}'\ \tilde{\varphi}\ \tilde{\varphi}']$ is introduced as follows:

$$\tilde{x}\left(\hat{t}\right) = x\left(\hat{t}\right) - x_{\text{ref}}\left(\hat{t}\right). \tag{84}$$

The total control scheme is shown in Fig. 7. The control law is composed of two terms as follows:

$$r_1\left(\hat{t}\right) = r_{1c}\left(\hat{t}\right) + r_{1f}\left(\hat{t}\right) \tag{85a}$$
$$r_2\left(\hat{t}\right) = r_{2c}\left(\hat{t}\right) + r_{2f}\left(\hat{t}\right) \tag{85b}$$

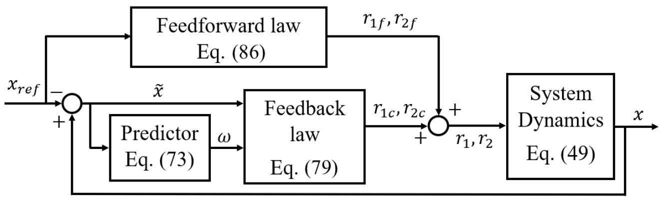

Fig. 7. Total closed-loop block diagram.

where r_{if}, $i = 1, 2$, are the feedforward terms to ensure that the desired trajectory is a solution of the closed-loop system

$$\begin{aligned} r_{1f}(\hat{t}) &= u''_{\text{ref}}(\hat{t}+\bar{h}_1) - \bar{A}u''_{\text{ref}}(\hat{t}-\bar{\tau}_1+\bar{h}_1) \\ &\quad + \bar{\psi}u_{\text{ref}}(\hat{t}+\bar{h}_1) + \bar{N}u'_{\text{ref}}(\hat{t}+\bar{h}_1) + \bar{Q}\varphi_{\text{ref}}(\hat{t}+\bar{h}_1) \\ &\quad - \bar{\psi}\bar{A}u_{\text{ref}}(\hat{t}-\bar{\tau}_1+\bar{h}_1) + \bar{A}\bar{N}u'_{\text{ref}}(\hat{t}-\bar{\tau}_1+\bar{h}_1) \\ &\quad - \bar{\psi}u_{\text{ref}}(\hat{t}-\bar{\tau}_3+\bar{h}_1) - \bar{Q}\varphi_{\text{ref}}(\hat{t}-\bar{\tau}_3+\bar{h}_1) \\ &\quad + \bar{\psi}\bar{A}u_{\text{ref}}(\hat{t}-\bar{\tau}_4+\bar{h}_1) \quad (86a) \\ r_{2f}(\hat{t}) &= \varphi''_{\text{ref}}(\hat{t}+\bar{h}_2) - A\varphi''_{\text{ref}}(\hat{t}-\bar{\tau}_2+\bar{h}_2) \\ &\quad + \psi u_{\text{ref}}(\hat{t}+\bar{h}_2) + Q\varphi_{\text{ref}}(\hat{t}+\bar{h}_2) + N\varphi'_{\text{ref}}(\hat{t}+\bar{h}_2) \\ &\quad - \psi A u_{\text{ref}}(\hat{t}-\bar{\tau}_2+\bar{h}_2) + AN\varphi'_{\text{ref}}(\hat{t}-\bar{\tau}_2+\bar{h}_2) \\ &\quad - \psi u_{\text{ref}}(\hat{t}-\bar{\tau}_3+\bar{h}_2) - Q\varphi_{\text{ref}}(\hat{t}-\bar{\tau}_3+\bar{h}_2) \\ &\quad + \psi A u_{\text{ref}}(\hat{t}-\bar{\tau}_5+\bar{h}_2) \quad (86b) \end{aligned}$$

which are designed such that

$$\begin{Bmatrix} 0 \\ r_{1f}(\hat{t}-\bar{h}_1) \\ 0 \\ r_{2f}(\hat{t}-\bar{h}_2) \end{Bmatrix} = x'_{\text{ref}}(\hat{t}) - \sum_{i=1}^{2} E_i x'_{\text{ref}}(\hat{t}-\bar{\tau}_i) - A_0 x_{\text{ref}}(\hat{t}) - \sum_{i=1}^{5} A_i x_{\text{ref}}(\hat{t}-\bar{\tau}_i). \quad (87)$$

Note that we use the fact that $x_{\text{ref}}(\hat{t})$ is known *a priori*, and hence, the delays in the control inputs as in (49) can be compensated for as far as the feedforward is concerned.

The terms r_{ic}, $i = 1, 2$, in (85) are given in (79), while here, $\tilde{x}$ [defined in (84)] is used in the feedback actions, and $\omega(\hat{t})$ is the estimate of the tracking error $\tilde{x}(\hat{t}+\hat{\tau}_p)$ [instead of $x(\hat{t}+\hat{\tau}_p)$].

Fig. 8 shows the spectrum of the prediction error dynamics (76) with $p_1 = p_2 = p_3 = p_4 = 0.01$. As depicted, all the characteristic roots lie in the LHP, which ensures the stability of the prediction error dynamics (76).

The prediction errors are shown in Figs. 9 and 10 for the axial and torsional dynamics, where $e_u(\hat{t}), e_{u'}(\hat{t}), e_\varphi(\hat{t})$, and $e_{\varphi'}(\hat{t})$ are the prediction errors of tracking errors $\tilde{u}(\hat{t}+\hat{\tau}_p), \tilde{u}'(\hat{t}+\hat{\tau}_p), \tilde{\varphi}(\hat{t}+\hat{\tau}_p)$, and $\tilde{\varphi}'(\hat{t}+\hat{\tau}_p)$, respectively. These figures depict an asymptotic convergence to zero prediction error for all prediction times for a given initial condition of the predictor [5% difference compared to $\tilde{x}(0)$]. Note that Figs. 9 and 10 are dimension-less.

By employing HANSO and PSO algorithms to design the controller gains, given in (69), the following controller gains

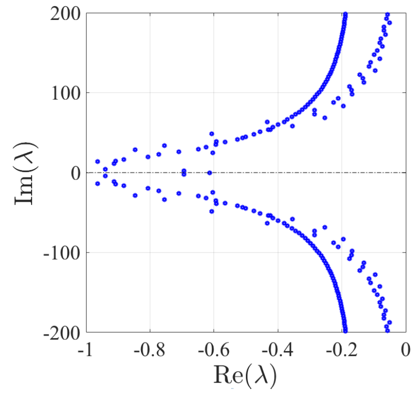

Fig. 8. Spectrum of the prediction error dynamics.

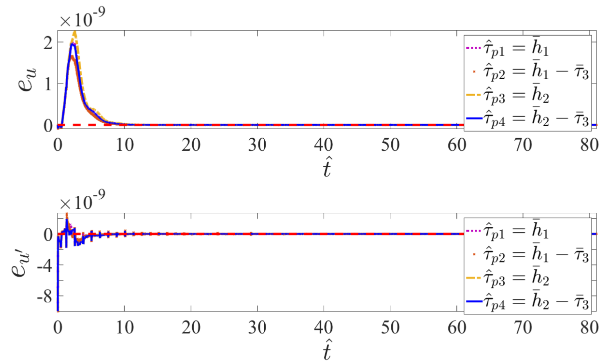

Fig. 9. Axial prediction errors for different prediction times.

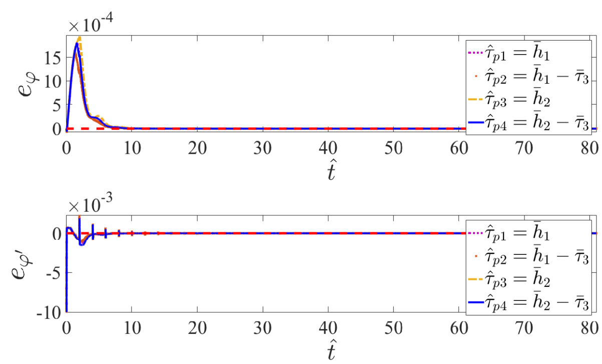

Fig. 10. Torsional prediction errors for different prediction times.

are obtained:

$$\begin{aligned} &k_1 = -994.4, \quad k_2 = -85.5, \ k_3 = -6.4 \times 10^{-6} \\ &k_4 = 9, \quad k_5 = 342.5, \ k_6 = 8.3 \times 10^{-4} \\ &k_7 = -9.1 \times 10^7, \quad k_8 = -3.5, \ k_9 = -78.7 \\ &k_{10} = -4.3, \quad k_{11} = 4.2 \times 10^7, \ k_{12} = 2.8 \end{aligned} \quad (88)$$

which leads to the closed-loop spectrum shown in Fig. 11. It illustrates that the closed-loop system is exponentially stable since all closed-loop characteristic roots lie in the LHP. Note that the vertical asymptotes of the spectrum remain unchanged since the controller does not affect the neutral terms. The latter fact emphasizes the importance of the formal stability analysis presented in Section IV.

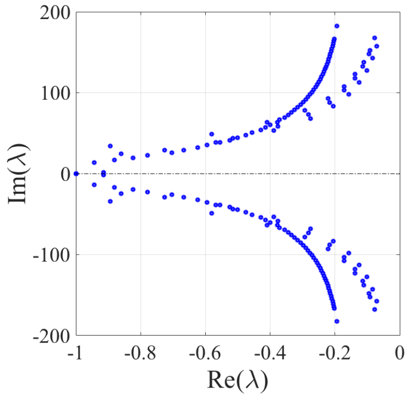

Fig. 11. Spectrum of the tracking error dynamics.

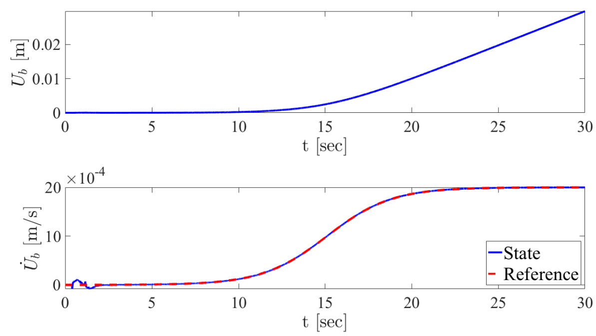

Fig. 12. Closed-loop axial behavior.

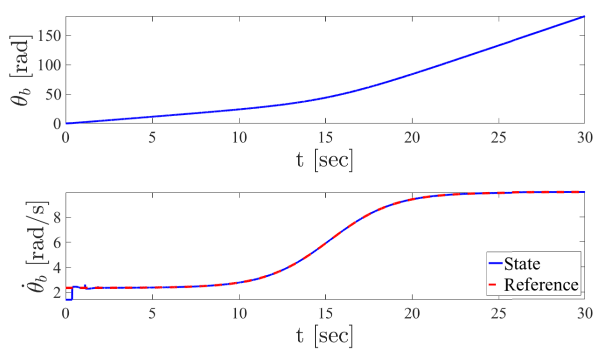

Fig. 13. Closed-loop angular behavior.

The closed-loop system behavior is shown in Figs. 12 and 13 for the axial and torsional dynamics, which shows that indeed the bit velocities track the desired references. Here, the bit is considered to have a zero axial velocity and 1.4 rad/s angular velocity for $-(2\tau_t + \tau_n) < t < 0$. As it can be seen in Figs. 12 and 13, the bit velocities are constant at the beginning ($\dot{U}_b = 0$ m/s and $\dot{\theta}_b = 1.4$ rad/s) since the control input waves have not reached the bit yet due to wave propagation delays. In particular, it takes time (equal to input delays) for the input waves, initiating at the top, to reach the bit at the bottom.

The physical control inputs, i.e., the velocity of the traveling block $V_{\rm TB}(t)$ and the top-drive torque $u_T(t)$, consist of transformed control inputs $u_1(t)$ and $u_2(t)$, and the contributions

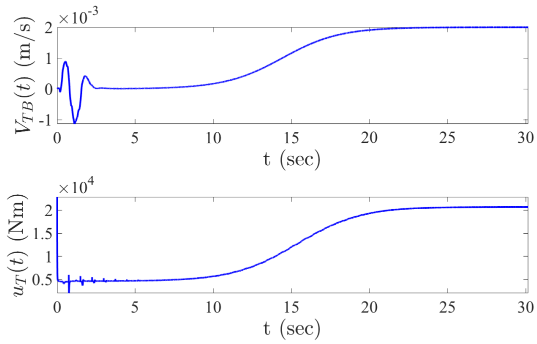

Fig. 14. Physical actuation variables.

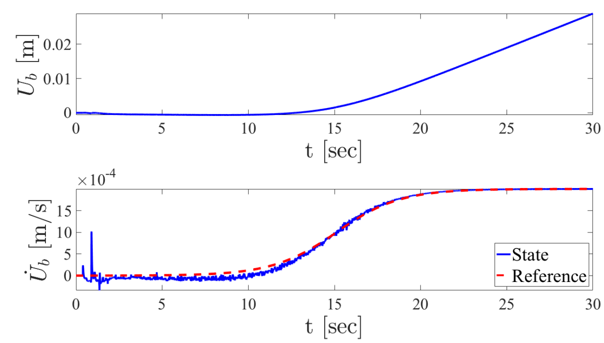

Fig. 15. Closed-loop axial behavior of the nonlinear system.

from the precompensators, which can be computed using the following relations:

$$\frac{\partial U_{\rm top}}{\partial s}(t) = c_a\left(\frac{\partial \mathbf{f}_a}{\partial \Upsilon_a}(t) - \frac{\partial \mathbf{g}_a}{\partial \Lambda_a}(t)\right) \tag{89}$$

where $(\partial \mathbf{f}_a)/(\partial \Upsilon_a)(t)$ and $(\partial \mathbf{g}_a)/(\partial \Lambda_a)(t)$ are given in (20), and

$$\frac{\partial^2 \theta_{\rm top}}{\partial t^2}(t) = \frac{\partial^2 \mathbf{f}_t}{\partial \Upsilon_t^2}(t) + \frac{\partial^2 \mathbf{g}_t}{\partial \Lambda_t^2}(t) \tag{90}$$

where $(\partial^2 \mathbf{f}_t)/(\partial \Upsilon_t^2)(t)$ and $(\partial^2 \mathbf{g}_a)/(\partial \Lambda_a^2)(t)$ can be obtained by differentiating (25). As shown in Fig. 14, in the steady-state motion, the feed rate $V_{\rm TB}$ is equal to the rate of penetration, i.e., 0.002 m/s. Moreover, the maximum value of the top-drive torque $u_T(t)$ is around 2×10^4 N·m, which is an acceptable value regarding the torque limitation of the top drive. Note that with significantly heavier top-drives, either the maximum value of the $u_T(t)$ may cross the acceptable limit or increased high-frequency contents in $u_T(t)$ might be observed.

Next, the designed controller is applied to the nonlinear system, given in (40). As it is shown in Figs. 15 and 16, the controller is able to deal with the state-dependent delay as well. The high-frequency behavior, which is observed in the axial dynamics (see Fig. 15), stems from the excitations of higher order modes of the axial drill-string dynamics that are inherent to the infinite-dimensional nature of these dynamics.

Note that in this simulation study, a white Gaussian noise has been added to the measured states, where the signal-to-noise ratio (SNR) has been considered as SNR $= 10$. Based on these results, it is concluded that the designed control

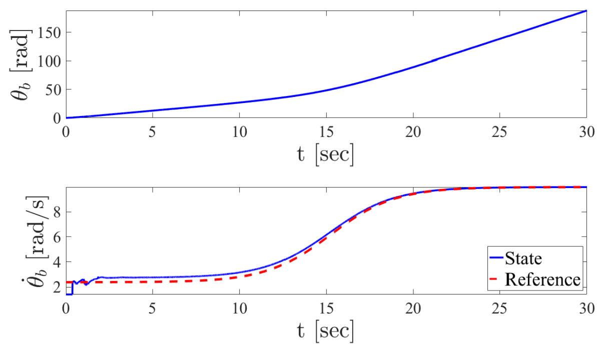

Fig. 16. Closed-loop angular behavior of the nonlinear system.

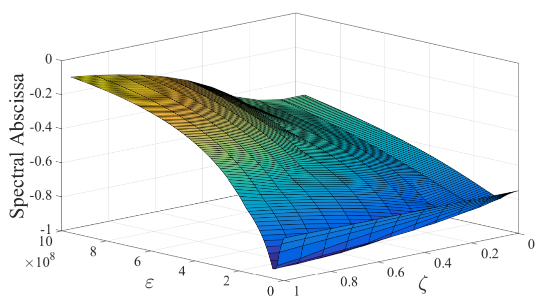

Fig. 17. Robust behavior in the presence of parametric uncertainties.

approach is robust against the measurement noise. Another source of uncertainty, which plays a role in the scope of the current work, is the parametric uncertainty, which is studied in Section VII-C.

C. Robustness Analysis Against Parametric Uncertainty

Drilling systems are subjected to different types of uncertainties. In the scope of the current work, the most important source of uncertainty is given by the parameters in the bit–rock interaction model (due to uncertainties in rock properties and bit wear) [74], [75]. Therefore, in this section, parametric uncertainty in the bit–rock interaction is considered in order to have a more realistic description of the system and to study the robustness of the designed controller. For this purpose, ζ (the cutter face inclination number) and ε (the rock intrinsic specific energy) in (14) are considered uncertain.

The variation of the closed-loop spectral abscissa for different values of the parameters ε and ζ is shown in Fig. 17 ($0 < \zeta < 1$ and $\varepsilon > 0$). As illustrated, the spectral abscissa remains negative for a wide range of these parameters. This feature, along with the formal stability of system, assures the robustness of the designed controller in terms of stabilizing the system while these parameters are uncertain. As shown in Fig. 18, with fixed ε and ζ varying between 0 and 1, the closed-loop spectral abscissa remains negative. However, with fixed ζ, the closed-loop will be unstable when $\varepsilon > 2.02 \times 10^9$ Pa which corresponds to an extremely hard rock formation. Note that we took the range on ε larger in Fig. 18 in comparison to Fig. 17 to find the critical value of ε that makes the closed-loop system unstable.

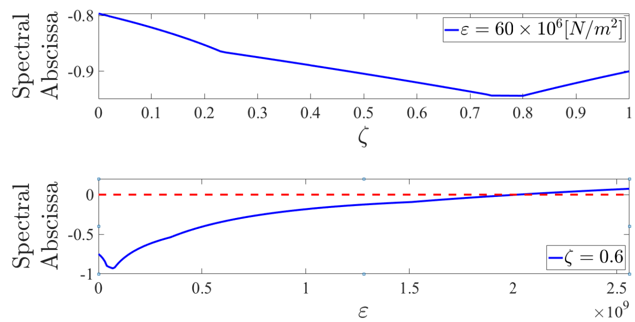

Fig. 18. Variation of spectral abscissa with (a) varying ζ and fixed ε and (b) varying ε and fixed ζ.

VIII. Conclusion

A distributed model has been employed to study the coupled axial–torsional vibrations in drilling systems. Here, first, both the cutting process and frictional contact have been taken into consideration in the bit–rock interaction, and second, realistic top-side boundary conditions are included. The resulting equations of motion are NDDEs with state-dependent state delays, constant state delays, and constant input delays. For the associated linear system, the stability has been analyzed by using a spectral approach to study the root causes of the steady-state vibrations and to serve as a basis for controller design. It is shown that the drilling system is intrinsically unstable but stabilizable by (delayed) state feedback. Under the premise of stabilizability, the optimization-based continuous pole-placement method has been employed to stabilize both axial and torsional dynamics, using the velocity of the traveling block and the top-drive torque as control inputs. The designed state-feedback controller deals with several time delays corresponding to the oscillatory behavior of the dynamics, and the bit–rock interaction. Moreover, it only employs top-side measurements. To make the controller causal, a state predictor with observer structure has also been designed. The effectiveness and robustness of both the controller and the predictor have been shown by illustrative simulation results.

References

[1] E. M. Navarro-López, "An alternative characterization of bit-sticking phenomena in a multi-degree-of-freedom controlled drillstring," *Nonlinear Anal., Real World Appl.*, vol. 10, no. 5, pp. 3162–3174, Oct. 2009.

[2] Y. Liu, J. P. Chávez, R. De Sa, and S. Walker, "Numerical and experimental studies of stick–slip oscillations in drill-strings," *Nonlinear Dyn.*, vol. 90, no. 4, pp. 2959–2978, Dec. 2017.

[3] Z. Huang, D. Xie, B. Xie, W. Zhang, F. Zhang, and L. He, "Investigation of PDC bit failure base on stick-slip vibration analysis of drilling string system plus drill bit," *J. Sound Vib.*, vol. 417, pp. 97–109, Mar. 2018.

[4] D. Bresch-Pietri and M. Krstic, "Adaptive output feedback for oil drilling stick-slip instability modeled by wave PDE with anti-damped dynamic boundary," in *Proc. ACC*, Jun. 2014, pp. 386–391.

[5] U. J. F. Aarsnes and N. van de Wouw, "Dynamics of a distributed drill string system: Characteristic parameters and stability maps," *J. Sound Vib.*, vol. 417, pp. 376–412, Mar. 2018.

[6] U. J. F. Aarsnes and N. van de Wouw, "Axial and torsional self-excited vibrations of a distributed drill-string," *J. Sound Vib.*, vol. 444, pp. 127–151, Mar. 2019.

[7] B. Saldivar, S. Mondié, J.-J. Loiseau, and V. Rasvan, "Stick-slip oscillations in oillwell drilstrings: Distributed parameter and neutral type retarded model approaches," *IFAC Proc. Volumes*, vol. 44, no. 1, pp. 284–289, Jan. 2011.

[8] I. Boussaada, H. Mounier, S.-I. Niculescu, and A. Cela, "Analysis of drilling vibrations: A time-delay system approach," in *Proc. 20th Medit. Conf. Control Autom. (MED)*, Jul. 2012, pp. 610–614.

[9] S. Tashakori, G. Vossoughi, H. Zohoor, and E. A. Yazdi, "Modification of the infinite-dimensional neutral-type time-delay dynamic model for the coupled axial–torsional vibrations in drill strings with a drag bit," *J. Comput. Nonlinear Dyn.*, vol. 15, no. 8, Aug. 2020.

[10] M. Krstic, *Delay Compensation for Nonlinear, Adaptive, and PDE Systems*. Cambridge, MA, USA: Birkhäuser Boston, 2009.

[11] B. Saldivar, S. Mondié, S.-I. Niculescu, H. Mounier, and I. Boussaada, "A control oriented guided tour in oilwell drilling vibration modeling," *Annu. Rev. Control*, vol. 42, pp. 100–113, 2016.

[12] N. Mihajlović, A. A. van Veggel, N. van de Wouw, and H. Nijmeijer, "Analysis of friction-induced limit cycling in an experimental drill-string system," *J. Dyn. Syst., Meas., Control*, vol. 126, no. 4, pp. 709–720, Dec. 2004.

[13] E. M. Navarro-López and E. Licéaga-Castro, "Non-desired transitions and sliding-mode control of a multi-DOF mechanical system with stick-slip oscillations," *Chaos, Solitons Fractals*, vol. 41, no. 4, pp. 2035–2044, Aug. 2009.

[14] T. Richard, C. Germay, and E. Detournay, "A simplified model to explore the root cause of stick–slip vibrations in drilling systems with drag bits," *J. Sound Vib.*, vol. 305, no. 3, pp. 432–456, Aug. 2007.

[15] X. Liu, N. Vlajic, X. Long, G. Meng, and B. Balachandran, "Nonlinear motions of a flexible rotor with a drill bit: Stick-slip and delay effects," *Nonlinear Dyn.*, vol. 72, nos. 1–2, pp. 61–77, Apr. 2013.

[16] X. Liu, N. Vlajic, X. Long, G. Meng, and B. Balachandran, "State-dependent delay influenced drill-string oscillations and stability analysis," *J. Vib. Acoust.*, vol. 136, no. 5, Oct. 2014, Art. no. 051008.

[17] B. Besselink, T. Vromen, N. Kremers, and N. van de Wouw, "Analysis and control of stick-slip oscillations in drilling systems," *IEEE Trans. Control Syst. Technol.*, vol. 24, no. 5, pp. 1582–1593, Sep. 2016.

[18] S. K. Gupta and P. Wahi, "Global axial–torsional dynamics during rotary drilling," *J. Sound Vib.*, vol. 375, pp. 332–352, Aug. 2016.

[19] S. K. Gupta and P. Wahi, "Criticality of bifurcation in the tuned axial–torsional rotary drilling model," *Nonlinear Dyn.*, vol. 91, no. 1, pp. 113–130, Jan. 2018.

[20] C. Germay, V. Denoël, and E. Detournay, "Multiple mode analysis of the self-excited vibrations of rotary drilling systems," *J. Sound Vib.*, vol. 325, nos. 1–2, pp. 362–381, Aug. 2009.

[21] C. Germay, N. Van de Wouw, H. Nijmeijer, and R. Sepulchre, "Nonlinear drillstring dynamics analysis," *SIAM J. Appl. Dyn. Syst.*, vol. 8, no. 2, pp. 527–553, Jan. 2009.

[22] B. Besselink, N. van de Wouw, and H. Nijmeijer, "A semi-analytical study of stick-slip oscillations in drilling systems," *J. Comput. Nonlinear Dyn.*, vol. 6, no. 2, Apr. 2011, Art. no. 021006.

[23] K. Nandakumar and M. Wiercigroch, "Stability analysis of a state dependent delayed, coupled two DOF model of drill-stringvibration," *J. Sound Vib.*, vol. 332, no. 10, pp. 2575–2592, May 2013.

[24] X. Liu, N. Vlajic, X. Long, G. Meng, and B. Balachandran, "Coupled axial-torsional dynamics in rotary drilling with state-dependent delay: Stability and control," *Nonlinear Dyn.*, vol. 78, no. 3, pp. 1891–1906, Nov. 2014.

[25] A. Depouhon and E. Detournay, "Instability regimes and self-excited vibrations in deep drilling systems," *J. Sound Vib.*, vol. 333, no. 7, pp. 2019–2039, Mar. 2014.

[26] U. J. F. Aarsnes and O. M. Aamo, "Linear stability analysis of self-excited vibrations in drilling using an infinite dimensional model," *J. Sound Vib.*, vol. 360, pp. 239–259, Jan. 2016.

[27] B. Saldivar, S. Mondié, J.-J. Loiseau, and V. Rasvan, "Exponential stability analysis of the drilling system described by a switched neutral type delay equation with nonlinear perturbations," in *Proc. 50th IEEE Conf. Decis. Control Eur. Control Conf. (CDC-ECC)*, Dec. 2011, pp. 4164–4169.

[28] T. Vromen *et al.*, "Mitigation of torsional vibrations in drilling systems: A robust control approach," *IEEE Trans. Control Syst. Technol.*, vol. 27, no. 1, pp. 249–265, Jan. 2019.

[29] T. Vromen, N. van de Wouw, A. Doris, P. Astrid, and H. Nijmeijer, "Nonlinear output-feedback control of torsional vibrations in drilling systems," *Int. J. Robust Nonlinear Control*, vol. 27, no. 17, pp. 3659–3684, 2017.

[30] C. Lu, M. Wu, X. Chen, W. Cao, C. Gan, and J. She, "Torsional vibration control of drill-string systems with time-varying measurement delays," *Inf. Sci.*, vol. 467, pp. 528–548, Oct. 2018.

[31] S. Tashakori and M. Fakhar, "Suppression of torsional vibrations in drilling systems by using the optimization-based adaptive backstepping controller," *Int. J. Mech. Control*, vol. 20, no. 1, pp. 105–110, 2019.

[32] D. Bresch-Pietri and M. Krstic, "Output-feedback adaptive control of a wave PDE with boundary anti-damping," *Automatica*, vol. 50, no. 5, pp. 1407–1415, May 2014.

[33] U. J. F. Aarsnes, F. Di Meglio, and R. J. Shor, "Avoiding stick slip vibrations in drilling through startup trajectory design," *J. Process Control*, vol. 70, pp. 24–35, Oct. 2018.

[34] M. B. Saldivar, S. Mondié, and J. J. Loiseau, "Reducing stick-slip oscillations in oilwell drillstrings," in *Proc. 6th Int. Conf. Electr. Eng., Comput. Sci. Autom. Control (CCE)*, Nov. 2009, pp. 1–6.

[35] C. Sagert, F. Di Meglio, M. Krstic, and P. Rouchon, "Backstepping and flatness approaches for stabilization of the stick-slip phenomenon for drilling," *IFAC Proc. Volumes*, vol. 46, no. 2, pp. 779–784, 2013.

[36] M. Barreau, F. Gouaisbaut, and A. Seuret, "Practical stability analysis of a drilling pipe under friction with a PI-controller," *IEEE Trans. Control Syst. Technol.*, vol. 29, no. 2, pp. 620–634, Mar. 2021.

[37] A. S. Yigit and A. P. Christoforou, "Stick-slip and bit-bounce interaction in oil-well drillstrings," *J. Energy Resour. Technol.*, vol. 128, no. 4, pp. 268–274, Dec. 2006.

[38] D. Bresch-Pietri and F. Di Meglio, "Prediction-based control of linear input-delay system subject to state-dependent state delay–application to suppression of mechanical vibrations in drilling," *IFAC-PapersOnLine*, vol. 49, no. 8, pp. 111–117, 2016.

[39] B. Saldivar, S. Mondié, and J. C. Á. Vilchis, "The control of drilling vibrations: A coupled PDE-ODE modeling approach," *Int. J. Appl. Math. Comput. Sci.*, vol. 26, no. 2, pp. 335–349, Jun. 2016.

[40] B. Saldivar, S. Mondié, J. J. Loiseau, and V. Rasvan, "Suppressing axial-torsional coupled vibrations in drillstrings," *J. Control Eng. Appl. Inform.*, vol. 15, no. 1, pp. 3–10, 2013.

[41] I. Boussaada, A. Cela, H. Mounier, and S.-I. Niculescu, "Control of drilling vibrations: A time-delay system-based approach," in *Proc. 11th Workshop Time-Delay Syst.*, 2013, pp. 226–231.

[42] B. Saldivar, T. Knüppel, F. Woittennek, I. Boussaada, H. Mounier, and S. I. Niculescu, "Flatness-based control of torsional-axial coupled drilling vibrations," *IFAC Proc. Volumes*, vol. 47, no. 3, pp. 7324–7329, 2014.

[43] S. Dwars *et al.*, "Recent advances in soft torque rotary systems," presented at the SPE/IADC Drilling Conf. Exhib., London, U.K., 2015.

[44] J. D. Jansen and L. van den Steen, "Active damping of self-excited torsional vibrations in oil well drillstrings," *J. Sound Vib.*, vol. 179, no. 4, pp. 647–668, Jan. 1995.

[45] E. Cayeux, "On the importance of boundary conditions for real-time transient drill-string mechanical estimations," presented at the IADC/SPE Drilling Conf. Exhib., Fort Worth, TX, USA, 2018.

[46] U. J. F. Aarsnes, O. M. Aamo, and M. Krstic, "Extremum seeking for real-time optimal drilling control," in *Proc. Amer. Control Conf. (ACC)*, Jul. 2019, pp. 5222–5227.

[47] J. J. Loiseau, M. Cardelli, and X. Dusser, "Neutral-type time-delay systems that are not formally stable are not BIBO stabilizable," *IMA J. Math. Control Inf.*, vol. 19, nos. 1–2, pp. 217–227, Mar. 2002.

[48] W. Michiels and S.-I. Niculescu, *Stability and Stabilization of Time-Delay Systems: An Eigenvalue-Based Approach*. Philadelphia, PA, USA: SIAM, 2007.

[49] W. R. Tucker and C. Wang, "On the effective control of torsional vibrations in drilling systems," *J. Sound Vib.*, vol. 224, no. 1, pp. 101–122, Jul. 1999.

[50] E. Kreuzer and M. Steidl, "Controlling torsional vibrations of drill strings via decomposition of traveling waves," *Arch. Appl. Mech.*, vol. 82, no. 4, pp. 515–531, Apr. 2012.

[51] U. J. F. Aarsnes, J. Auriol, F. Di Meglio, and R. J. Shor, "Estimating friction factors while drilling," *J. Petroleum Sci. Eng.*, vol. 179, pp. 80–91, Aug. 2019.

[52] J. J. Bailey and I. Finnie, "An analytical study of drill-string vibration," *J. Eng. Ind.*, vol. 82, no. 2, pp. 122–127, May 1960.

[53] I. Finnie and J. J. Bailey, "An experimental study of drill-string vibration," *J. Eng. Ind.*, vol. 82, no. 2, pp. 129–135, May 1960.

[54] D. Bresch-Pietri and M. Krstic, "Adaptive output-feedback for wave PDE with anti-damping–application to surface-based control of oil drilling stick-slip instability," in *Proc. 53rd IEEE Conf. Decis. Control*, Dec. 2014, pp. 1295–1300.

[55] T. Insperger, G. Stépán, and J. Turi, "State-dependent delay in regenerative turning processes," *Nonlinear Dyn.*, vol. 47, nos. 1–3, pp. 275–283, Dec. 2006.

[56] F. Hartung, “Linearized stability for a class of neutral functional differential equations with state-dependent delays,” *Nonlinear Anal., Theory, Methods Appl.*, vol. 69, nos. 5–6, pp. 1629–1643, Sep. 2008.

[57] W. Michiels, “Spectrum-based stability analysis and stabilisation of systems described by delay differential algebraic equations,” *IET Control Theory Appl.*, vol. 5, no. 16, pp. 1829–1842, Nov. 2011.

[58] W. Michiels. *TDS-Stabil: A MATLAB Tool for Fixed-Order Stabilization Problems for Time-Delay Systems*. [Online]. Available: http://twr.cs.kuleuven.be/research/software/delay control/stab

[59] W. Michiels and S.-I. Niculescu, “Stability, control, and computation for time-delay systems,” in *An Eigenvalue-Based Approach. Advances in Design and Control*, vol. 27, 2nd ed. Philadelphia, PA, USA: SIAM, 2014.

[60] C. I. Byrnes, M. W. Spong, and T.-J. Tarn, “A several complex variables approach to feedback stabilization of linear neutral delay-differential systems,” *Math. Syst. Theory*, vol. 17, no. 1, pp. 97–133, Dec. 1984.

[61] *HANSO: Hybrid Algorithm for Non-Smooth Optimization*. [Online]. Available: https://cs.nyu.edu/overton/software/hanso/

[62] J. V. Burke, A. S. Lewis, and M. L. Overton, “A robust gradient sampling algorithm for nonsmooth, nonconvex optimization,” *SIAM J. Optim.*, vol. 15, no. 3, pp. 751–779, Jan. 2005.

[63] R. Poli, J. Kennedy, and T. Blackwell, “Particle swarm optimization,” *Swarm Intell.*, vol. 1, no. 1, pp. 33–57, Jun. 2007.

[64] V. L. Kharitonov, “An extension of the prediction scheme to the case of systems with both input and state delay,” *Automatica*, vol. 50, no. 1, pp. 211–217, Jan. 2014.

[65] B. Zhou, “Input delay compensation of linear systems with both state and input delays by nested prediction,” *Automatica*, vol. 50, no. 5, pp. 1434–1443, May 2014.

[66] V. L. Kharitonov, “Predictor based stabilization of neutral type systems with input delay,” *Automatica*, vol. 52, pp. 125–134, Feb. 2015.

[67] V. L. Kharitonov, “Prediction-based control for systems with state and several input delays,” *Automatica*, vol. 79, pp. 11–16, May 2017.

[68] B. Zhou and Q. Liu, “Input delay compensation for neutral type time-delay systems,” *Automatica*, vol. 78, pp. 309–319, Apr. 2017.

[69] S. Mondié and W. Michiels, “Finite spectrum assignment of unstable time-delay systems with a safe implementation,” *IEEE Trans. Autom. Control*, vol. 48, no. 12, pp. 2207–2212, Dec. 2003.

[70] V. L. Kharitonov, “Predictor-based controls: The implementation problem,” *Differ. Equ.*, vol. 51, no. 13, pp. 1675–1682, Dec. 2015.

[71] G. Besancon, D. Georges, and Z. Benayache, “Asymptotic state prediction for continuous-time systems with delayed input and application to control,” in *Proc. Eur. Control Conf. (ECC)*, Jul. 2007, pp. 1786–1791.

[72] V. Léchappé, E. Moulay, and F. Plestan, “Dynamic observation-prediction for LTI systems with a time-varying delay in the input,” in *Proc. IEEE 55th Conf. Decis. Control (CDC)*, Dec. 2016, pp. 2302–2307.

[73] I. Estrada-Sánchez, M. Velasco-Villa, and H. Rodríguez-Cortés, “Prediction-based control for nonlinear systems with input delay,” *Math. Problems Eng.*, vol. 2017, pp. 1–11, Oct. 2017.

[74] T. G. Ritto, C. Soize, and R. Sampaio, “Non-linear dynamics of a drill-string with uncertain model of the bit–rock interaction,” *Int. J. Non-Linear Mech.*, vol. 44, no. 8, pp. 865–876, Oct. 2009.

[75] T. G. Ritto and R. Sampaio, “Stochastic drill-string dynamics with uncertainty on the imposed speed and on the bit-rock parameters,” *Int. J. Uncertainty Quantification*, vol. 2, no. 2, pp. 111–124, 2012.

Shabnam Tashakori was born in 1990. She received the Ph.D. degree in mechanical engineering from the Sharif University of Technology, Tehran, Iran, in 2019.

She was a Visiting Researcher with the Eindhoven University of Technology, Eindhoven, The Netherlands, in 2018. She is currently the Chair of Management Board (COB) with Raha, Tehran, startup company, and a Founding Member of the Rahesh Innovation Center, Shiraz, Iran. Her current research interests include (non)linear dynamics and control with applications in the drilling industry and impact force reconstruction.

Gholamreza Vossoughi received the Ph.D. degree from the Department of Mechanical Engineering, University of Minnesota, Minneapolis, MN, USA, in 1992.

Ever since, he joined the Faculty of Mechanical Engineering, Sharif University of Technology, Tehran, Iran. He was the Director of the Manufacturing Engineering and Applied Mechanics Division, the Graduate Dean and the Chairman of the Department of Mechanical Engineering, and the Dean of Graduate Studies at the Sharif University of Technology. His research interests include bio-inspired robotics, microrobotic systems, man–machine interface, exoskeletal and haptic systems, mechatronics, and control systems. He has published more than 100 peer-reviewed journal articles in these fields.

Hassan Zohoor was born in 1945. He received the Ph.D. degree from Purdue University, West Lafayette, IN, USA, in 1978.

He was the Founder, the President, and a Developer of principal codes and regulations at Payame Noor University, Tehran, Iran; the Acting President of Al-Zahra University, Tehran; and the President of Shiraz University, Shiraz, Iran. He spent his post-doctoral time at Purdue University. He is currently an Academician of the IR Iran Academy of Sciences (IAS) and a Professor Emeritus at the Sharif University of Technology, Tehran, Iran. He is also the Head of the Higher Education Committee, Iranian National Commission for UNESCO. He is the author or the coauthor of over 550 scientific articles and holds five patents. He has supervised over 220 graduate theses. He was assigned as the Coordinator of the Preamble Section of the Mentioned Drafting Committee from 2016 to 2017.

Dr. Zohoor received the Mustafa Prize, the Award of Distinguished Professor in the IR Iran in 1993, the Lasting Personalities Award in Iran in 2001, and the Allameh Tabatabaei Award, special award of National Elite Foundation, in 2013. He has been elected as an expert by UNESCO, Asia Pacific Region, and appointed as a member of the Drafting Committee of a Global Convention on the Recognition of Higher Education Qualifications at UNESCO since 2016. He has been the Chair of the Scientific Committee since 2014, and a Section Editor of *Scientia Iranica* (Transaction B, Previous Elsevier Editorial System). He was the Secretary of the IAS.

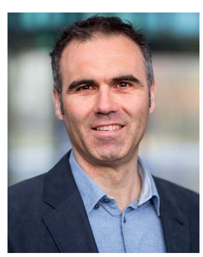

Nathan van de Wouw (Fellow, IEEE) was born in 1970. He received the M.Sc. (Hons.) and Ph.D. degrees in mechanical engineering from the Eindhoven University of Technology, Eindhoven, The Netherlands, in 1994 and 1999, respectively.

He was with Philips Applied Technologies, Eindhoven, and the Netherlands Organization for Applied Scientific Research, Delft, The Netherlands, in 2000 and 2001, respectively. He was a Visiting Professor at the University of California at Santa Barbara, Santa Barbara, CA, USA, from 2006 to 2007, The University of Melbourne, Melbourne, VIC, Australia, from 2009 to 2010, and the University of Minnesota, Minneapolis, MN, USA, from 2012 to 2013. He is currently a Full Professor with the Department of Mechanical Engineering, Eindhoven University of Technology, and an Adjunct Full Professor with the University of Minnesota. He has authored a large number of journal and conference papers and the books *Uniform Output Regulation of Nonlinear Systems: A Convergent Dynamics Approach* with A. V. Pavlov and H. Nijmeijer (Birkhauser, 2005) and *Stability and Convergence of Mechanical Systems with Unilateral Constraints* with R. I. Leine (Springer-Verlag, 2008).

Dr. van de Wouw was a recipient of the IEEE Control Systems Technology Award for the development and application of variable-gain control techniques for high-performance motion systems in 2015. He is also an Associate Editor of *Automatica* and the IEEE TRANSACTIONS ON CONTROL SYSTEMS TECHNOLOGY.